Reducing the Amount of M1 Microglia by Inhibiting CXCR4 and iNOS Exerts Neuroprotection in a Rat Model of Subarachnoid Hemorrhage

Wenhao Qu
First Affiliated Hospital of Soochow University
Ying Cheng
Soochow University Medical College
Wei Peng
First Affiliated Hospital of Soochow University
Tongyu Rui
Soochow University Medical College
Chengliang Luo
Soochow University Medical College
Jian Zhang (yxbati@163.com)
First Affiliated Hospital of Soochow University https://orcid.org/0000-0002-5684-7345

Research Article

Keywords: subarachnoid hemorrhage, microglia migration, ferroptosis, lipid peroxidation, neuroinflammation, neuroprotection

Posted Date: September 7th, 2021

DOI: https://doi.org/10.21203/rs.3.rs-856199/v1

Abstract

Early inflammation is a significant factor in acute pathophysiological events of early brain injury (EBI) after subarachnoid hemorrhage (SAH). Although there have been numerous studies of neuroinflammation and SAH, the effect of M1 microglia on the progressions of neuroinflammation in SAH remains non-elucidated. CXCR4 is thought to be the critical regulator of the migration and recruitment of microglia, and early studies found that iNOS/NO• does represent an effective ferroptosis regulator and leads to the M1 microglia more resistant to the initiator of ferroptosis. Thus, we investigated the effect of AMD3100 (a highly selective antagonist of CXCR4) and L-NIL (an inhibitor of iNOS) on neuroinflammation in a rat SAH model. We found AMD3100 could suppress the migration of M1 microglia through the CXCL12/CXCR4 pathway. Treatment of AMD3100 could decrease the level of related inflammation factors and improved the prognosis within 24 h after SAH. Moreover, L-NIL could inhibit the expression of (i)NOS and promote the expression of ferroptosis-related proteins and the degree of lipid peroxidation. Importantly, the combination of AMD3100 and L-NIL could reduce the quantity of M1 microglia in the injured brain area and reduce the secretion of related inflammatory factors to improve the prognosis. To sum up, these data indicate that inhibiting CXCR4 and iNOS following SAH produces cerebral protection, and its anti-inflammation provides a potential therapeutic target for treating SAH.

Introduction

Subarachnoid hemorrhage (SAH) is a severe form of stroke accounting for high mortality and morbidity [1]. The main cause of SAH is rupture of an intracranial aneurysm, covering approximately Eighty-five percent of SAH [2]. Despite the advances in disease management, the mortality rate rises to 30% in acute situations. In recent years, early brain injury (EBI), occurring within the first 72 hours after aneurysmal SAH, is an essential contributor to the poor outcome after SAH. EBI contains numerous pathophysiological events: inflammation, brain edema, increased blood-brain barrier (BBB) permeability, apoptosis, and neurodegeneration [3]. Early inflammation is a significant factor in acute pathophysiological events. Within several hours after SAH, the inflammatory response is rapidly initiated, and various inflammatory cells, especially microglia, flock to the damaged cerebral parenchyma. Then, various proinflammatory cytokines are expressed from microglia and lead to severe damage to the brain [4]. Therefore, attenuating SAH-induced inflammation may have great benefits in alleviating neurological damage and improving the prognosis.

Microglia cells, considered as innate immune cells of the central nervous system (CNS) widely, are one of the major cellular components that induce neuroinflammation. Microglia can be rapidly activated by pathological stimulation of the CNS. When the CNS is destroyed, microglia can be activated to remove apoptotic cells, damaged tissue and cell debris, tissue metabolites as well as contribute to repairing damaged nervous system. Whereas, continuously activated microglia secrete plenty of inflammatory mediators such as TNF-α, IL-1β, reactive oxygen species (ROS) and reactive nitrogen species (RNS), etc., thus impairing mitochondrial function, resulting in neuronal degeneration and necrosis, and further exacerbating CNS damage [5]. According to reports that microglia are classified into a classic pro-

inflammatory (phenotypes M1) and an alternative anti-inflammatory (phenotypes M2) [6, 7]. M1 microglia typically expresses proinflammatory molecules, such as TNF-a, IL-6, IL-1β and iNOS, which can exacerbate inflammation [8, 9]. M2 microglia mainly secrete factors that exert anti-inflammatory and neuroprotective effects, such as IL-10, IL-4, TGF-b, BDNF, and NGF [8, 10]. It has been found that the number and activation of M1 microglia after SAH is one of the most significant factors causing neuroinflammation after EBI [11]. It could be the main reason of early brain injury after SAH. However, in early brain injury, the mechanism of changes in the number of M1 microglia in the damaged brain parenchyma remains to be determined.

Early studies suggested that the microglia of rodents express CXCR4 (CXC chemokine receptor 4) [12–14]. CXCR4 and its ligand CXCL12 (CXC motif chemokine ligand 12) are thought to be the critical regulator of the migration and recruitment of microglia [15, 14]. Naturally, we can put forward a hypothesis that inhibiting CXCR4 at the early brain injury of SAH may reduce the microglia migration to reduce the number of microglia in the damaged brain parenchyma attenuate the inflammatory.

Ferroptosis is a redox-driven cell death program [16, 17], which is the result of getting out of control over three programs—iron metabolism, lipid peroxidation, and thiol regulation. The regulatory metabolic basis of the cell death program contains the (phospho) lipid hydroperoxides which are Fe-dependent generation, and the ability of their reduction to alcohols through glutathione peroxidase 4 (GPX4) [18]. GPX4 prevents the degradation of hydroperoxy lipids to the oxidatively truncated reactive electrophilic species [19, 20] that attacks some as-yet-undefined critical protein targets, resulting in cell demise [21, 22].

Early studies found that iNOS/NO• does represent an effective ferroptosis regulator and leads to the macrophages and M1 microglia is highly resistant to the initiator of ferroptosis. On the contrary, the lack of iNOS in the M2 phenotype showed high sensitivity to the stimulation of pro-ferroptosis [23]. Thus, we reasonably wondered whether inhibition of iNOS / NO• leads to the ferroptosis of M1 microglial at the early brain injury of SAH, thereby reduces the number of M1 microglia to attenuate the inflammatory.

In the present study, we used the SAH model in rats and OxyHb-induced BV-2 cells model to investigate (1) the effect of the CXCR4/CXCL12 pathway on M1 microglia migration and proinflammatory cytokine production, (2) the effect of inhibiting iNOS / NO• on the expression of ferroptosis related proteins and degree of lipid peroxidation, and (3) whether promoting the ferroptosis of M1 microglia to further reduce the amount of M1 microglia base on inhibiting the migration of M1 microglia could attenuate the inflammation after the acute phase of SAH and improve long-term outcomes after SAH.

Material And Methods

Animals

All animal procedures were approved by the Ethics Committee of the First Affiliated Hospital of Soochow University and conformed to the guidelines of the National Institutes of Health on the care and use of

animals. Adult male Sprague-Dawley rats weighing between 300 and 350 g were purchased from the Animal Center of Chinese Academy of Sciences, Shanghai, China. Placed all animals in a humidified room with a constant temperature of (24 ± 2) °C, air humidity (50 ± 10%), and under a 12-h light/dark cycle, and free to food and water. All of the rats were placed under an aesthesia before the fixation-perfusion and exsanguination euthanasia procedures. Try our best to minimize the number of experimental animals and their suffering.

Rat SAH Model

As a previous study [24] described, 10% chloral hydrate (0.4 ml/kg) was injected intraperitoneally to anesthetized those rats and fix all the rats in the stereotaxic apparatus. The experimental SAH model consisted of a needle with a rounded tip and a side hole stereotaxic insertion into the prechiasmatic cistern. The needle was at an angle of 45 degrees to the sagittal plane and was inserted 7.5 mm anterior to the bregma with the needle side hole facing the right side. The final depth of the needle tip was 2–3 mm anterior to the chiasma (about 10–12 mm from the surface of the brain), then retracted 0.5 mm. If needed, use bone wax to plug the burr hole to prevent loss of CSF and blood from the midline vessels prior to needle insertion. Following this, 0.3 ml non-heparinized autologous arterial blood from the femoral artery was slowly delivered into the prechiasmatic cistern for 20 seconds under aseptic conditions using a syringe pump. For control, inject 0.3 ml saline into the sham group of rats by using the same method. To prevent dehydration of those rats, 20 ml of 0.9% saline were subcutaneously injected after the SAH procedures immediately. After recovering for about 45 min, return all rats to their cages, maintain the room temperature at 23 ± 1°C. Meanwhile, we monitored the heart rate and rectal temperature of the rats and maintained the rectal temperature at 37 ± 0.5°C during the experiments. Then at the indicated time point after experimental SAH, rats were euthanized. It was observed in this study that the inferior basal temporal lobe was stained by blood. Next, we collected the brain tissues surrounding the hemorrhage located in the temporal base and subjected them to analysis. We used the underlying temporal base brain tissues alone for western blot analysis and the total coronal sections containing temporal base brain tissues for immunofluorescence analysis, Prussian blue reaction, and FJB staining. The collected tissue area is shown in Fig. 1.

Drug Administration

AMD3100, which was applied as CXCL12/CXCR4 antagonist extensively [25–27], was used in this study to restrain CXCR4. AMD3100 (Plerixafor 8HCl, JM3100 octahydrochloride) was obtained from Sigma-Aldrich (St. Louis, MO, USA), dissolved into DMSO (the final concentration: 0.5%), then diluted to the final injection concentration by 0.9% physiological saline. AMD3100 (1 mg/kg) was administered by intraperitoneal (i.p.) injection 1 h after SAH. The dosage of the time of administration and the dosage of AMD3100 were chosen based on previous studies [28] and have been proven to be effective. The vehicle (0.5% DMSO in saline) was administered to the rats 1 h after SAH.

L-N (6)-iminoethyl-lysine (L-NIL) (Sigma, St. Louis, MO, USA), an inducible (i) NOS inhibitor, was dissolved in DMSO (the final concentration: 0.5%), then diluted to the final injection concentration by 0.9%

physiological saline. L-NIL (20 mg/kg, 0.3 mL i.p) was injected after 6 h post-trauma. The dosage of the time of administration and the dosage of L-NIL was chosen according to pharmacokinetic studies [29] and has been proven to be effective. The vehicle (0.5% DMSO in saline) was administered to the rats 15 min and 12 h after SAH.

Liproxstatin-1 (Lip-1), a potent and specific inhibitor of ferroptosis, was purchased from TargetMol. It was dissolved in DMSO (the final concentration: 0.5%), then diluted to the final injection concentration by 0.9% physiological saline. The inhibitor was then administered to the rats at the doses of 5 mg/kg via intraperitoneal injection at 2 h before the induction of SAH. The dose of Lip-1 was chosen based on a previous study [30] and has been proven to be effective. The vehicle (0.5% DMSO in saline) was administered to the rat 2 h after SAH.

Experimental Design

Part 1. Probe the change of CXCR4 and CXCL12 expression and the time pattern of change after SAH, and the tendency of the number of different types of microglia in the damage zone of Brain parenchyma after each time point after SAH. Rats were divided into seven groups randomly, and then euthanized according to the indicated time points after the induction of SAH: sham, 1 h, 6 h, 12 h, 24 h, 48 h, 72 h. The rats were anesthetized by 10% chloral hydrate (3.5 ml/kg) deeply at each specific time point after SAH. Five rats per group were sacrificed, and then transcranial perfused using chilled PBS. The brain tissues were collected from the temporal lobe base, stored at − 80℃ immediately, and then used for Western blotting.

Part 2. Probe the mechanism of M1 microglia migration in vitro and the effect of AM3100 on the prognosis of SAH rats. The mechanism of the migration of M1 microglia is probed by performing the transwell migration assay. BV2 microglia, treated with LPS for 24 h, polarized into M1 phenotype. M1 microglia was seeded in the chamber at appropriate densities. The experiment was performed with the following groups: (1) Vehicle (2) AMD3100 (3) CXCL12 (4) AMD3100 and CXCL12. The ability of migration of M1 microglia was quantified by viewing the cell number in four different fields at a microscope, at least in triplicate. Elisa assay and the neurobehavioral experiment were performed to evaluate the prognosis. For the Elisa assay, rats were divided into three groups: sham, SAH, and SAH + AMD3100. Collect serum from each rat to measure the expression of related inflammation factors at different time points, at least in triplicate. For the neurobehavioral experiment, the wire-grip test and the Morris water maze test have proceeded. The recovery of neurobehavioral was assessed by specific indicators (each group set contained 6 samples; n = 6; Fig. 1c).

Part 3. Probe the relation between ferroptosis and M1 microglia. OxyHb induced BV2 cells to mimic an in vitro model of SAH. The cells were divided into 6 groups randomly: Normal, OxyHb, OxyHb + DMSO, OxyHb + DMSO + L-NIL, OxyHb + DMSO + Lip-1, OxyHb + DMSO + L-NIL + Lip-1. Western blot, malondialdehyde (MDA) content and lipid peroxidation (Lipid-ROS) assay were evaluated at the specific time after OxyHb was induced (Fig. 1c).

Part 4. Probe the relation between the quantity of microglia and the degree of neuroinflammation, neuronal damage, behavioral deficits, and functional recovery after the early stage of SAH. Rats were divided into five groups: Sham, SAH + Vehicle, SAH + AMD3100, SAH + L-NIL, SAH + ADM3100 + L-NIL, injected vehicles, or drugs by intraperitoneal injection. To observe the amount of M1 microglia, we performed the Western blot assay and the immunofluorescence staining (each group set contained 5 samples; n = 5). To detect the tendency of inflammatory factors such as IL-6, TNF-α, IL-1β at the specific time point after SAH, we collected the serum of experimental rats performed for ELISA (each group set contained 5 samples; n = 5). To evaluate the degree of neuronal damage, we performed Nissl staining and Fluoro-Jade B (FJB) staining (each group set contained 5 samples; n = 5). In order to assess the degree of behavioral deficits and functional recovery of the early stage of SAH, the Wire-grip test and the Morris Water Maze test were evaluated at indicated time-points after SAH (each group set contained 6 samples; n = 6; Fig. 1c).

Western Blot Analysis

Western blot analysis was carried out by using standard procedures as previously described. The animals were anesthetized deeply via intraperitoneal injection using 10% chloral hydrate, and animals were sacrificed after anesthesia. We took out the tissues of the temporal-floor brain after perfusing the brain tissue transcardially with 150 ml of chilled PBS. Homogenize the samples by using RIPA lysis buffer and then sonicate them. We collected the supernatant after centrifuging the homogenates at 12000 × g at 4°C for 20 minutes. The protein concentrations were measured by using the A280 method with NanoDrop 2000C (Thermo Scientific, USA). Equal quantified sample (30 μg) was loaded for 7.5% − 15% SDS-PAGE then electrophoresed with a semidry electrotransferred unit for transferred to polyvinylidene fluoride membranes. At room temperature, blocking membranes were performed with 5% skim blocking grade milk for 2 hours. The diluted primary antibodies were incubated with membranes overnight at 4°C: CXCR4, CXCL12, iNOS, CD206, CD86, Tfr1, Tf, COX2, xCT, Fth, Ftl, GPX4, GAPDH, Tubulin. Membrane washing was performed three times with TBST after primary antibody incubation. The appropriate proportion of secondary antibodies was incubated with membranes (RT, 2h). The protein density of bands was captured by an ECL system (ChemiScope, Shanghai) after washing three times with TBST. Quantification of the Western blots was performed by using Image J software (NIH), and standardization was done with GAPDH or Tubulin.

Transmigration Assay

The ability of cell migration is analyzed by using a transwell system (aperture of 8 μm;24-well insert; Millipore, USA). Place the 200 μl cell solution. The concentration is 1.5×10^5 cells/mL and contains AMD3100 (2.5 μl /mL) or vehicle, in the upper chamber. Place the 600 μl medium containing CXCL-12 (200ng/ml, Beyotime Biotechnology, Shanghai) or vehicle in the lower chamber. In another independent experiment, the lower chamber was seeded with the astrocytes that were exposed to 10 μM OxyHb (Jinpin Chemical Technology, China) to mimic SAH condition as reported previously. After 16 hours of incubation at 37°C, cells were fixed using 4% paraformaldehyde solution (RT, 1h). Then the non-migrate cells of the top of the upper chamber are removed by gently scrubbing with cotton swabs. The 0.1% crystal violet

purchasing from Santa Cruz Biotechnology, Inc. (Santa Cruz, CA) is used to stain the migrated cells for 10 mins, and the count of cells is performed with Olympus LCX100 Imaging system (Olympus Corporation, Tokyo, Japan). All experimental results were performed independently, at least in triplicate.

Immunofluorescence Staining

Brains were removed and fixed using 4% paraformaldehyde (24h), then brains were rapidly frozen and cut into 10-mm thick coronal slices. Frozen slices were air-dried and were rehydrated in PSB. Then slices were permeabilized with blocking buffer (PBS with 10% BSA and 0.3% Triton) for 2 h. Subsequently, these slices were incubated at 4°C overnight with the following primary antibodies: CXCR4/CXCL12/I-BA1. The appropriate proportion of secondary antibodies (Beyotime Biotechnology, Shanghai) was incubated with slices (RT, 1h after washing three times with PSB. To observe the cell density of total cells, nuclear staining of these slices was carried out with 4', 6-diamidino-2-phenylindol (DAPI, Beyotime Biotechnology, Shanghai), and then slices were observed using the fluorescence microscope.

Perls' Prussian Blue Staining

The iron accumulation was detected with Perls' Prussian blue stain, as described previously [31]. After washing three times with PBS, the brain slices were permeabilized with PBS containing 0.3% Triton (RT, 5 mins). Subsequently, these slices were incubated with Perl's reagent (equal parts 5% hydrochloric acid and 5% potassium ferrocyanide) for 30 mins. Then slices were washed in PSB three times rightly again. To inactivated endogenous peroxidase activity, brain slices were covered with 0.3% hydrogen peroxide (H_2O_2) in methanol for 15 minutes and then were washed in PBS three times lastly. Then slices were incubated in 3, 3-diaminobenzidine (DAB) to develop(□□□develop) immunoreactive signals and used hematoxylin to counterstaining.

Lipid Peroxidation Assay

The BV-2 cells were induced by LPS to acquired M1 polarization characteristics. The working solution of BODIRY 581/591 C11(10 μM) was used to co-incubate with the M1 microglia cells. The fluorescence changed from red to green as lipid peroxidation increases.

Malondialdehyde (MDA) Content

The lipid peroxidation MDA assay kit (#S0131S, Beyotime Biotechnology, Shanghai, China) was used following the manufacturer's instructions to measure the microglia malondialdehyde (MDA) content. In brief, the cells were collected and homogenized with a cold lysis solution. The lysates were then centrifuged at 12,000 g for 10mins at 4°C to collect the supernatant. The MDA solution (200 μL) was added to each sample or supernatant (0.1 mL). The mixture was then heated at 100°C for 15 min and collected supernatant after centrifuged at 1000 g for 10 min after cooled to room temperature in the water bath. The supernatant (200 μL) was colorimetrically quantified (Thermo Scientific Multiskan FC, OD = 532 nm). MDA levels were expressed as nmol/mg.

Nissl Staining

For Nissl staining, the coronal brain sections were fixed in 4% formaldehyde and washed with PSBT 3 times. The Nissl staining solution purchased from Beyotime Biotechnology (Shanghai, China) was used to incubate with each brain section (10min, 50℃). The microscope (Nikon TE300; Nikon) was used to capture five regions randomly for quantification to evaluate the peri-injury zone positively stained cells. Compared with normal neurons, we can observe shrunken and/or contained multiple vacuoles and darker color in nuclei stain.

Fluoro-Jade B (FJB) Staining

Whole brains were frozen and made as frozen sections (coronal sections of 10 μm thickness). Then the sections were fixed with 4% paraformaldehyde for 24 h. Fluoro-Jade B (FJB) staining was performed based on the instructions provided by the manufacturer (Millipore, Germany). Firstly, the basic alcohol solution, which was made up of 1% sodium hydroxide and 70% ethanol, was used to immerse the coronal brain sections for 5 minutes. Then the sections were rinsed in 70% ethanol for 2minutes and were washed in distilled water for 2 minutes. Potassium permanganate solution (0.06%) was then used to immerse those tissues for 10 minutes. Subsequently, the specimens of slides were incubated in a Fluoro-Jade B solution (0.0004%) for 30 minutes after 2 minutes of distilled water rinse. The microscope (Nikon TE300, Japan) was used to observe the captured images. Measure and quantify the count of Fluoro-Jade B-positive cells in three sections per rat.

M1 Microglia Polarization and a SAH Model *in Vitro*

The murine microglial BV2 cell line (BeNa Culture Collection, BNCC337749) was cultivated in Dulbecco's modified Eagle's medium (DMEM; Gibco™ GlutaMAX™) containing 10% fetal bovine serum (FBS; Gibco), penicillin (100 U/mL), and streptomycin (100 μg/mL). The cells were cultured in a humidified incubator maintained at 37°C containing 5% CO2 and were passaged once every 3 days. Then the lipopolysaccharides (LPS, 1 μg/ml), Sigma-Aldrich) were added to the BV2 cell line to polarize microglia to M1[32].

In mimic the experimental SAH in vitro, the cells were cultivated in Petri dishes until the density of cells reached 80%-90%, and then the medium was replaced with a serum-free medium. The cells were stimulated with oxyhemoglobin (OxyHb, Sangon Biotech) for 6 h. The appropriate duration (6h) of stimulation was obtained through the CCK8 assay.

Primary Culture

The primary astrocytes were obtained from the brain tissue of 1- to 2-day-old Sprague–Dawley rats as previously reported [33]. The rat pup's brain tissue was taken out and removed the blood vessels and meninges from the cortices. Wash the brain cortex with PBS and digest with 0.25% trypsin (37℃, 5min). Then complete DEME/F12 medium, containing 10 % FBS, 2 mM of L-Glutamine100 mM of nonessential amino acids, 1 mM of sodium pyruvate, 50 U/ml of penicillin/streptomycin was used to terminate trypsinization. Resuspend the cells with complete DMEM/F12 medium after centrifugation. Cell

suspension was added in petri dishes. The oligodendrocytes and microglial cells were separated from astrocytes by gently shaken at 210rpm at 14 days after initial seeding. The astrocytes were seeded in a 24-well plate at a density of 5×10^5/well. Then cells were stimulated with OxyHb for 6h and were prepared for transwell assay.

The cortex of 1-d-old neonatal rats was prepared to perform primary cultures of cortical neurons. We dissected the neonatal rats' cortices and cultured them in Neurobasal-A medium (Gibco) with 2% B27 (Gibco), 100 U/mL penicillin, and 100 μg/mL streptomycin (Gibco). Then the cell suspension was plated on a Poly-D-lysine-coated (0.1 mg/mL, Sigma) 96-well plate at the density of 1×10^4cells/cm^2 for 6–8 days to perform the experiments as follows.

Cell Viability Assay

The microglia cells were seeded into a 96-well plate at the density of 1x104 cells/well and incubated for 72h with or without the stimulation with OxyHb. The cells were incubated for 1hours in the dark at 37℃ after adding 10 μl Cell Counting Kit-8 (CCK8) reagents (Dojindo, Kumamoto, Japan) to per well. The absorbance of each well was measured at a wavelength of 450 nm by a microplate reader (Bio-Rad, Hercules, CA).

Enzyme-Linked Immunosorbent Assay (ELISA)

The content of the related factors of inflammation was detected using the corresponding ELISA kit (Beyotime Biotechnology, Shanghai). Briefly, the standard products and the tested samples were diluted in a particular proportion, then add them into the enzyme-labeled plate for 2 h at 37°C. Then we removed the solution and washed the enzyme-labeled plate 5 times with the washing buffer. The biotinylated antibody was added and incubated with each enzyme-labeled plate (RT, 1h). Remove the solution and wash the enzyme-labeled plate 5 times again. Add the horseradish peroxidase in plates to mark streptavidin at RT for 20 mins, protect from light. Remove the solution and wash the enzyme-labeled plate 5 times lastly. The color development was achieved with 3, 3, 5, 5-tetramethylbenzidine (TMB) after washing. Stopped solution was added to terminate the reaction. The OD of each plate was measured immediately at 450 nm in a microplate reader (Thermo, MA, USA) and was recorded.

Wire-grip Test and Morris Water Maze (MWM)

The grip strength of animals was assessed by using the wire-grip test. The test was performed as previously described [34, 35]. A 40cm wire was suspended tightly between two upright bars at the height of 50cm above a table. Grasp the rats’ tail and place rats on the wire so that rats grasp the wire with both front paws, and observe the following to evaluate the grip strength: the time length of rats remaining on the wire (0-60s), the way of holding on (paw and tail). The final score of each rat about the wire grip test was obtained through an average of three trials.

To evaluate the impact of AMD3100 and L-NIL on the memory performance of rats after SAH, the Morris Water Maze (MWM) test was performed on days 8–16 post-SAH, as previously described. Three days before SAH, rats were trained in the standard MWM three times per day. Each rat was permitted 60s (cut-

off time) to reach the hidden platform and stayed on it for 15 s during each trial. If a rat is unable to reach the platform in 60 s, it is permitted to be guided to it for staying for 15 s. The time of each rat to reach the platform (swimming escape latency) was recorded automatically, and the analysis was carried out by using video/compute tracking software.

Brain Water Content Measurement

The wet weight / dry weight method was conducted to evaluate brain edema [36]. The animals were euthanized and decapitated immediately at 24 hours after SAH. Brains were divided into four parts immediately. They respectively are cerebellum, brainstem and left and right cerebral hemispheres. Wet weight was obtained firstly. Then the brain specimens were dried in an oven at 100°C for 72 hours and then dry weight was obtained. The percentage of water content was calculated by using the following formula: ([wet weight - dry weight]/wet weight) ×100% [37].

Neurobehavioral

The 18-point Modified Garcia test and the beam balance test were used to evaluate neurobehavioral deficits blindly at 24 hours after SAH. 6 tests consist of Garcia Score [38] including spontaneous activity (in the cage for 5 min); the symmetry of all four limbs to move; symmetry of forelegs outstretching (outstretching while held by the tail); climbing wall of wire cage; body proprioception after trunk touch; and response to vibrissae stimulation. The score of each test ranged from 0 to 3. The total score is between 3 withe 18 (3 worst and 18 best). The beam balance was performed by putting rats on a cramped wooden beam to walk for 1 minute. The rats obtained 3 points for walking distance ≥ 20 cm; the rats obtained 2 points for walking distance < 20 cm; the rats obtained 1 point for walking distance < 10 cm, and the rats falling before the distance of walking < 10 cm obtained 0 points.

Statistical Analyses

Statistical analyses were performed using GraphPad Prism 8 Software (San Diego, CA, USA). The student's t-test (two-tailed, unpaired) was performed for experiments with only two groups. Statistical analyses were carried out using an ANOVA (one-way or two-way) to compare with more than two groups, followed by a post hoc Tukey test. All P values were two-sided, and statistical significance was set at the level of $P < 0.05$.

Results

CXCR4 and CXCL12 Expression Was Upregulated after SAH

As introduction mention demonstrated that CXCR4 was expressed from rodent microglia. The pathway CXCR4/CXCL12 (CXCL12 is the ligand of CXCR4) is the critical factor of the migration and recruitment of microglia. In the SAH rats, we collected the brain tissues from the base of the temporal lobe for western blot to analyze the expression of CXCR4 at 1 h, 6 h, 12 h, 24 h, 48 h, 72 h after SAH. Results showed that the expression of CXCR4 increased gradually after SAH, and the peak elevation occurred at 12 h. Then, it presented a downward trend ($^{**}P < 0.01$ and $^{***}P < 0.001$; Fig. 2b). Meanwhile, we offered another result

within 72 h after SAH that compared with the sham group. The expression of CXCL12, the ligand of CXCR4, increased gradually, with the peak at 12 h, then it followed a decreasing trend ($^{**}P < 0.01$ and $^{***}P < 0.001$; Fig. 2c).

The Amount of M1 Microglia Increased and May Peak 24 h after SAH.

Previous studies showed that M1 polarization microglia could express marks (CD86, iNOS, and IL-1β) and release pro-inflammation factors (TNF-α and IL-6) [39, 40]. And CD206 and IL-10 are the special marker and expression factors respectively of M2 polarization microglia [10, 41, 42]. We divided the animals into seven groups according to the specific time point after the SAH model: sham, 1 h, 6 h, 12 h, 24 h, 48 h, 72h. Western blot was performed using the brain tissues to observe the expression levels of CD86, iNOS, and CD206. The result showed the expression of CD86 and iNOS had a rising tendency, and the peak elevation occurred at 24 h. Within 72 h after SAH, the expression level of CD206 of the experiment group had a gradually increasing trend compared with the sham group ($^{*}P < 0.05$, $^{**}P < 0.01$ and $^{***}P < 0.001$; Fig. 2). Our results suggest that the amount of M1 microglia may peak 24 h after SAH.

CXCR4/CXCL12 Was the Critical Pathway of the Migration of M1 Microglia.

We then performed the transwell experiment in vitro to explore the exact role of the CXCL12/CXCR4 pathway in the migration of M1 microglia. It is known that LPS can activate microglia polarize to M1. Firstly, we used LPS to induce BV2 microglia for 24 h for polarizing cells into the M1 phenotype. The merged image of the immunostaining for Iba-1 and iNOS carried out that LPS induced most of the BV2 cells to M1 (Fig. 3a). Additionally, the protein level of the biomarkers (CD86 and iNOS) of M1 microglia was detected by Western blot assay. The expression of CD86 and iNOS increased after LPS induced (Fig. 3b). The above results validate that the BV-2 microglia acquired M1 polarization characteristics by LPS induced.

To imitate the SAH model, the M1 microglia (LPS-induced BV-2 microglia) was exposed under oxyhemoglobin for 6 h. In this study, AMD3100 was the highly selective antagonist of CXCR4.AMD3100 or vehicle was added into the upper chamber, and CXCL12 or vehicle was added into the lower chamber. Then transwell assay was conducted on the four groups. When both chambers were added vehicle, only a small amount of M1 microglia could be migrated to the opposite surface of the transwell insert, while less M1 microglia migrated to the insert surface when AMD3100 was added to the upper chamber. Conversely, when we added CXCL12 into the lower chamber, more M1 microglia migrate to the surface. In the final group, CXCL12 was added into the lower chamber. Meanwhile, the AMD3100 was added into the upper chamber. We observed the migration of M1 microglia induced by CXCL12 was inhibited by AMD3100 ($^{**}P < 0.001$; Fig. 3c).

Previous studies found that the expression of CXCL12 increased after the brain injury [43]. The results of the previous assay that CXCL12 had an increasing trend after SAH also confirmed this point. In the CNS, CXCL12 was produced mainly by activated astrocytes [44–46]. Thus, we cultured and seeded the primary astrocytes in the lower chambers, which were induced by oxyhemoglobin to imitate the in vitro SAH

environment. The result of the transwell assay showed that in comparison with the control treatment group, the oxyhemoglobin-induced astrocytes could induce the migration of M1 microglia, and the migration phenomenon was significantly inhibited by AMD3100 ($^{**}P < 0.001$; Fig. 3d).

AMD3100 (an antagonist of CXCR4) Alleviated SAH-induced Inflammation and Improved the Outcome.

Elisa assay was performed to explore the expression level of related inflammation factors after AMD3100 treatment. We divided rats into three groups: sham, SAH, and SAH + AMD3100. Serum samples of each rat were collected for ELISA at 12 h, 24 h, 48 h, and 72 h after SAH modeling. The result showed that AMD3100 did not affect the sham group. Importantly, we found that the expression of inflammatory factor (IL-6, IL-1β, TNF-α), secreted by M1 microglia, had a decreased trend after the AMD3100 treatment compared with the vehicle group. However, we found the expression of the above factors had not significantly different from the vehicle group when SAH rats were treated by AMD3100 later than 24 h ($^{*}P < 0.05$, $^{**}P < 0.01$ and $^{***}P < 0.001$; Fig. 4).

To explore the effect of AMD3100 on the prognosis of SAH rats,we performed a series of behavioral experiments. In wire-grip test, we found that the rats of treatment group had a better score than the SAH group ($^{\#}P < 0.05$, $^{\#\#}P < 0.01$ and $^{\#\#\#}P < 0.01$; $^{**}P < 0.01$ and $^{***}P < 0.001$; Fig. 4d). We then performed the Morris water maze test when the muscle strength of the experimental group was not significantly different from that of the sham group. The SAH rats with AMD3100 treated had a shorter latency as the Fig. 4 shows ($^{\#}P < 0.05$ and $^{\#\#}P < 0.01$; $^{**}P < 0.01$ and $^{***}P < 0.001$; Fig. 4e). The above experiment proves that AMD3100 could alleviate the SAH-induced inflammation and improve the outcome.

Inhibition of Inducible NO Synthase/NO• Promoted Ferroptosis in M1 Microglia.

M1 microglia is a major microglia-type in the ischemic boundary zone within the first 72 h post-stroke [47]. We performed Perls' Prussian blue staining to observe the ferroptosis in the tissues of the temporal-floor brain. The outcomes showed no obvious higher level of non-heme iron in the temporal-floor brain within the first 48 h after the SAH model. Then the level increased significantly at 72 h and showed a gradual upward trend (Fig. 5a). This outcome was in line with that the M1-polarized microglia that were highly resistant to ferroptosis, and M2-polarized microglia were highly sensitive to ferroptosis stimulation.

As we stated before, three programs were included in the cell death program of ferroptosis: iron metabolism, lipid peroxidation, and thiol regulation—the related proteins of these programs like Tfr1, Tf, Fth, Ftl, xCT, GPX4. Moreover, COX2 is a well-recognized biomarker of ferroptosis [48]. BV2 cells were used for the Vitro experiment, and We examined the expression level of the protein associated with ferroptosis by performing the western blot assay. L-NIL and Lip-1 were used to treat, respectively. Our western blot result revealed that compared with the normal group, the expression of Tfr1, Tf, Fth, Ftl, and Cox2 presented an increasing tendency after induced OxyHb while the expression of GPX4 and xCT with a trend toward decrease ($^{\#}P < 0.05$, $^{\#\#}P < 0.01$, and $^{\#\#\#}P < 0.001$; Fig. 6). Compared with the vehicle group, protein expression of Tfr1, Tf, Fth, Ftl, and Cox2 showed a rising trend with the L-NIL treated, the GPX4

and xCT expression decreased. The result of Lip-1 treated group showed the opposite trend ($^{*}P < 0.05$, $^{**}P < 0.01$, and $^{***}P < 0.001$; Fig. 6).

As mentioned above, lipid peroxidation is associated with ferroptosis. C11-bodipy581 = 591 is very suitable for ratio fluorescence imaging of reactive oxygen species in living cell membranes. Figure 5b showed that OxyHb promoted lipid peroxide formation with the red fluorescence shifted to green fluorescence of the BODIPY, indicating the lipid peroxidation rises after OxyHb induced. We also found that L-NIL facilitated the significant upregulation of lipid peroxidation following OxyHb induced. Significantly, treating L-NIL-treated microglia cells with Lip-1could reduce BODIRY-C11 oxidation following OxyHb induced (Fig. 5b).

The MDA content of M1 microglia increased after being induced by OxyHb. The trend was made more evident after L-NIL treatment, while Lip-1 inhibited the increase in MDA content ($^{\#}P < 0.05$, $^{\#\#}P < 0.01$, and $^{\#\#\#}P < 0.001$; $^{*}P < 0.05$, and $^{**}P < 0.01$; Fig. 5c).

To sum up, these data suggest that OxyHb resulted in ferroptosis of M1 Microglia while L-NIL promotes this cell death program.

Reduced Quantity of M1 Microglia Alleviated Inflammation after Early Brain Injury.

According to previous studies, the expression levels of Cd86 and iNOS ref lected the M1 polarization of microglia and the count of M1 microglia correspondingly. To validate the effect of AMD3100 and L-NIL on the count of M1 microglia, we performed the following experiments. The rats were categorized into 5 groups: (1) Sham, (2) Vehicle, (3) Vehicle + AMD3100, (4) Vehicle + L-NIL and (5) Vehicle + AMD3100 + L-NIL. Then after 24 h's successful modeling, rats were euthanized. The brain tissues were used for Western blot. The result showed CD86 and iNOS had a significant rise tendency after SAH. The expression of CD86 and iNOS had a decreasing tendency when AMD3100, L-NIL, or both two drugs were administered ($^{\#}P < 0.05$, $^{\#\#}P < 0.01$ and $^{\#\#\#}P < 0.01$; $^{**}P < 0.01$ and $^{***}P < 0.001$; Fig. 7). Hence, these data indicated that AMD3100 and L-NIL treatment could decrease the count of M1 microglia after SAH.

To further investigate the effect of AMD3100 or L-NIL on the amount of M1 microglia in the temporal-floor brain after SAH, we detected M1 marker (iNOS) co-expression with microglia marker Iba-1 at 24 h after SAH. We found the amount of M1 microglia (Merge /Iba-1+) increased significantly at 24 h after SAH. Importantly, the amount of M1 microglia decreased with AMD3100 and/or L-NIL treatment ($^{*}P < 0.05$, $^{**}P < 0.01$ and $^{***}P < 0.001$; Fig. 7e). The result further confirmed that the AMD3100 and L-NIL treatment could decrease the amount of M1 microglia after SAH.

The inflammation factors in the sera of rats were detected using the specific ELISA kits to confirm the effect of AMD3100 and L-NIL on reducing the inflammation. TNF-α, IL-6, and IL-1β are the classic inflammation factors. Figure 8 showed that the level of inflammation factors of the vehicle group presented a significant upward tendency compared with the sham group. The expression level of inflammation factor compared with vehicle group had a decreasing trend after treatment with AMD3100

and L-NIL ($^{**}P < 0.01$ and $^{***}P < 0.001$; Fig. 8). These results further demonstrated that AMD3100 and L-NIL could alleviate inflammation after SAH.

Both AMD3100 and L-NIL Attenuated Neuronal Damage in SAH-induced Injury Brain Area

To further investigate the role of AMD3100 and L-NIL in neuronal damage following SAH. We conducted a series of experiments: Nissl staining and Fluoro-Jade B (FJB) staining. In Nissl staining, compared with the living neurons in the sham group, the cell bodies of damaged neurons exhibited cytoplasmic shrunken or nuclear fragments following SAH. After AMD3100 and L-NIL treatment, these histopathological changes were alleviated (Fig. 8f). We also performed FJB staining to determine neuronal degeneration after SAH. We found that SAH resulted in the number of degenerating neurons increased in damaged brain areas. The quantity of degenerating neurons of AMD3100 and L-NIL treatment group reduced obviously compared with the vehicle SAH group ($^{**}P < 0.01$ and $^{***}P < 0.001$; Fig. 8d). The above results showed both AMD3100 and L-NIL could prevent neuronal damage in the SAH-induced injury brain area.

Both AMD3100 and L-NIL Attenuated Neurological Dysfunctions and Brain Edema after SAH

To evaluate the effect of AMD3100 and L-NIL on neurobehavioral functions and brain edema after SAH. In neurobehavioral functions test, there were no significant differences between each group before SAH. Compared with the sham group, the neurological score of the animals in the vehicle group significantly decreased. We also got the observation that the neurobehavioral was markedly improved when the post-SAH animals were treated with AMD3100 and L-NIL. The result of the neurological score was given in the figure below ($^{*}P < 0.05$, $^{**}P < 0.01$; Fig. 9a).

In the brain edema test, both the animals of sham and experiment group were euthanasia 24 h after SAH. We found the brain edema of 24 h post-SAH animals increased significantly by 0.58% in the left hemisphere ($^{\#\#}P < 0.01$), 0.54% in the right hemisphere ($^{\#\#}P < 0.01$), and 0.30% ($^{\#\#}P < 0.01$) in the cerebellum compared with the animals of sham groups, while no change was observed in the brain stem. Our result also showed that the brain water content in the left and right hemisphere decreased after the treatment with AMD3100 or L-NIL (in the left hemisphere, AMD3100, 79.32 ± 0.11 vs. Vehicle, 79.61 ± 0.08, $^{*}P < 0.05$; L-NIL, 79.42 ± 0.08 vs. Vehicle, 79.61 ± 0.08, $^{*}P < 0.05$; in the right hemisphere, AMD3100, 79.29 ± 0.11 vs. Vehicle, 79.47 ± 0.06, $^{*}P < 0.05$; L-NIL, 79.38 ± 0.03 vs. Vehicle, 79.47 ± 0.06, $^{*}P < 0.05$), the same result was observed in the cerebellum (AMD3100, 79.09 ± 0.05 vs. Vehicle, 79.18 ± 0.04, $^{**}P < 0.01$; L-NIL, 79.12 ± 0.07 vs. Vehicle, 79.18 ± 0.04, $^{*}P < 0.05$;). The post-SAH animals which were treated with both AMD3100 and L-NIL had a significantly improved trend in the evaluation of brain edema. The brain water content of treated animals decreased significantly compared with the vehicle group (in the left hemisphere, AMD3100 and L-NIL, 79.20 ± 0.10 vs. Vehicle, 79.61 ± 0.08, $^{**}P < 0.01$; in the right hemisphere, AMD3100 and L-NIL, 79.09 ± 0.09 vs. Vehicle, 79.47 ± 0.06, $^{**}P < 0.01$; in the cerebellum, AMD3100 and L-NIL, 79.08 ± 0.07 vs. Vehicle, 79.09 ± 0.05, $^{**}P < 0.01$; Fig. 9b).

Both AMD3100 and L-NIL Decreased SAH-induced Brain Behavioral Deficits in Rats

To explore the effect of AMD3100 and L-NIL on SAH-induced neurological outcome, we performed two experiments: wire-grip test and Morris Water Maze (MWM). Animals used for experiment analysis were the same. Animals were divided into five groups: Sham, Vehicle + SAH, AMD3100 + SAH, L-NIL + SAH, AMD3100 + L-NIL + SAH. The wire-grip test was performed on days 1–7 firstly, and then we tested the Morris Water Maze (MWM) test on days 8–16 post-SAH (n = 7; Fig. 9c). Regarding the wire-grip test, the post-SAH animals had a significantly declined tendency on days1-7 compared with those in the sham group. But the motor performance of the animals treated with AMD3100 and L-NIL was ameliorated compared with those in the vehicle-treated SAH group (For Vehicle group: $^{**}P < 0.01$, $^{***}P < 0.001$ vs Sham group; for AMD3100 group: $^{\#}P < 0.05$, $^{\#\#}P < 0.01$, and $^{\#\#\#}P < 0.001$ vs Vehicle SAH group; for L-NIL group: $^{\&\&}P < 0.01$, $^{\&\&\&}P < 0.001$ vs Vehicle SAH group. for AMD3100 and L-NIL group: $^{\$}P < 0.05$, $^{\$\$}P < 0.01$, and $^{\$\$\$}P < 0.001$vs Vehicle SAH group; Fig. 9d). In the MWM test, the time of the animal found the platform was recorded. The shorter time means better learning and memory function. We observed that the post-SAH animals had an increased latency compared with the animals in the sham group on days 8–16. The animals treated with AMD3100 and L-NIL both displayed a shorter escape latency significantly than the vehicle-treated SAH animals (Fig. 9e).

Discussion

Early studies have demonstrated that brain damage following stroke, including SAH, is strongly associated with inflammation [49–51]. An extensive data of clinical have linked early inflammation in SAH to poor neurological outcomes [52]. The neuroinflammatory response that SAH resulted in including the phenotype of various CNS cells (astrocytes, neurons, and microglia) from endogenous and the influx of several leukocytes from the periphery (neutrophils, macrophages, and T-cells). Microglia, as the resident immune cells in the CNS, has versatile effectors. Microglia may polarize into two phenotypes under ischemic conditions: M1 phenotype, which could secrete proinflammatory cytokines and contribute to tissue damage, and M2 phenotype, which could phagocytose debris to repair tissue [53]. Selective regulation of different phenotypes microglia quantity and function could be an effective strategy to improve outcomes after SAH.

This study found that the microglia, particularly the M1 phenotype microglia, increased rapidly several hours after SAH. The primary sources of M1 microglia include the activation of resident microglia and chemotaxis from surrounding brain tissue [54]. The M2 phenotype microglia increased slowly in the beginning and then increased significantly at 24 h after SAH. Thus, the measures to reduce the quantity of M1 microglia in the early phase of SAH may be effective in alleviating the inflammation injury subsequently.

Our study showed that the expression of CXC motif chemokine ligand 12 (CXCL12) increased post-SAH. Moreover, we performed the transwell assay in vitro, and the assay demonstrated that the migration of M1 microglia could be induced by CXCL12 in vitro, and the AMD3100, the antagonist of CXCR4, could inhibit the tendency of migration effectively. This experiment suggested that the M1 microglia migration was mediated by CXCL12/CXCR4 signaling pathway. Then, in vivo experiment, rats were injected with

AMD3100 at different timepoints after SAH, and we detected the expression level of the inflammation factor of M1 phenotype microglia to confirm whether disturbing CXCL12/CXCR4 pathway could cause inhibit M1 phenotype microglia recruitment to the brain injury area and reduce the inflammation factor. We found that the expression of the specific inflammation secretion (IL-6, IL-1β, TNF-) of M1microglia had a decreasing tendency after AMD3100 treatment within 24 h after SAH. However, when SAH rats were treated by AMD3100 later than 24 h, M1 phenotype microglia had been abundantly recruited into the brain injury area, and we found the expression of the above factors had not significantly different from the vehicle group (Fig. 3). The benefit of AMD3100 could not be achieved. As previous studies mentioned, AMD3100 could inhibit the migration of M2 microglia after ischemia, and the effect of the inhibition increased 48 h after ischemia. And the previous studies even found that the enhanced neurogenesis and behavioral recovery were abrogated by consecutive infusing for 14 days with AMD3100 [55–58]. We further performed neurobehavioral experiments. Rats were divided into sham group, SAH group, and treatment group to perform wire-grip test and morris water maze test on consecutive seven days. The result showed that improvements in neurobehavior in the treatment group compared to the SAH group. Consequently, our study may support the idea that inhibiting the CXCRL12/CXCR4 pathway reduces M1 microglia recruitment and inflammation in the early brain injury to improve the prognosis and highlights the importance of an effective therapeutic time window for this pathway.

Based on the above results, we naturally wondered whether further reduce the amount of M1 microglia in the early brain injury could further alleviate inflammation and improve prognosis. Kapralov Alexandr A et al. [23] found that iNOS/NO• is a potent regulator of ferroptotic death. This feature leads the M1 polarized microglia to have a high resistance to ferroptosis. Conversely, the M2 polarized microglia, which lacks iNOS, displayed a heightened sensitivity to ferroptotic death. Notably, this sensitivity from pro-ferroptosis stimulation was abolished entirely when exogenously NO• donors were added. Iron metabolism, lipid peroxidation, and thiol regulation have been considered fundamental parts of ferroptosis. In iron metabolism, the free Fe3 + in peripheral blood combined with transferrin (Tf) is extracellular, and the complex binds with the transferrin receptor 1 (Tfr1) on the cell membrane. The Fe^{3+} were transported into the cell with the complex by endocytosis and reduced into Fe^{2+} with the effect of the six-transmembrane epithelial antigen of the prostate 3 (STEAP3). Then the Fe^{2+} was transferred to the cytosol at the Divalent Metal Transporter 1 (DMT1) mediated. The Fe^{2+} could be stored in the Ferritin, a spherical polymer consisting of ferritin heavy (Fth) and light (Ftl) chains and tight connection with ferroptosis or pump out from the cell with the Ferroportin, which is on the cell membrane. The homeostasis of iron in the cell was achieved in these two ways. The amounts of intracellular Fe^{2+} are excessive by an external stimulus and lead to the production of lipid ROS with the Fenton reaction. Then, the constant accumulation of lipid ROS could cause ferroptosis (Fig. 10). GPX4, an antioxidant enzyme, could degrade hydrogen peroxide (H2O2) and lipid ROS into H2O and corresponding alcohols with the assistance of glutathione (GSH). This function is essential for the cell to avoid oxidant injuries and is vital for cell survival [59]. GSH is an indispensable cofactor for GPX4 to operate. The cysteine is transported into the cell by cystine–glutamate transporter (system XC–), and meanwhile, the glutamate is carried out from the cell. The cystine in the cytosol transformed to cysteine (Cys), and the latter plays an essential role in GSH

synthesis [60]. The content of Cys in intracellular decrease due to blocked transport of cystine resulted in the synthesis of GSH reduced. Then the loss of GPX4 activity led to the accumulation of lipid ROS resulting in ferroptosis (Fig. 10b) [16].

Therefore, we performed in vitro experiments to detect the ferroptosis-associated factors of M1 microglia. In vitro experiment, the protein expression (Tf, Tfr1, Fth, Ftl), associated with iron metabolism, increased after SAH modeling. This trend was inhibited by a recognized inhibitor (Lip-1) of ferroptosis. Notably, the L-NIL, the inducible (i) NOS inhibitor, reversed this inhibition and even promoted the expression. For the regulatory pathways of GPX4. The expression level of GPX4 and xCT decreased after SAH was induced. L-NIL further reduces the expression of xCT and GPX4. And the decrease in xCT caused the decline in the transport of cystine which ultimately results in a significant reduction of GPX4. Ferroptosis occurred with the substantial accumulation of lipid ROS due to the decrease of GPX4. We also confirmed that the ferroptosis marker Ptgs2/COX2 (prostaglandin-endoperoxide synthase 2) [61] increased after SAH, and the L-NIL led to this tendency more significantly. It is well known that lipid peroxidation is an essential process of ferroptosis. The content of Malondialdehyde (MDA), a lipid peroxidation marker, is measured to assess the degree of lipid peroxidation[62]. The result showed that L-NIL promoted the degree of lipid peroxidation of M1 microglia while the degree of lipid peroxidation of M1 microglia was alleviated when treated with LIP-1. More importantly, we found that the results after two drugs were treated together were similar to the consequence treated with Lip-1 lonely. Similar effects were observed in C11-BODIPY581/591 (an alternative to detecting lipid peroxide formation[63]). The above results indicate that the L-NIL, the inducible (i) NOS inhibitor, may promote the ferroptosis of M1 microglia and thus reduces its amount. We even venture to guess that LIP-1 can resist the facilitation of L-NIL, but the exact mechanics will need to be explored further in the future.

We naturally wondered whether promoting ferroptosis in M1 microglia based on based on inhibiting M1 microglia migration would lead to a better prognosis. The results showed that the number of M1 microglia after being treated with both AMD3100 and L-NIL is less than using one agent only, and the inflammation factors are significantly decreased. Notably, we also observed better outcomes in the group treated with both agents.

The conclusion is that reducing the quantity of M1 microglia in the early brain injury (EBI) may produce cerebral protection in a rat SAH model. The conclusion is based on three key findings. First, the number of microglia was reduced by inhibiting migration via the CXCL12/CXCR4 pathway. Second, the L-NIL increased the susceptibility of microglia to ferroptosis via inhibiting iNOS, which, in turn, reduced the number of M1 microglia. Finally, a decrease in the number of M1 microglia resulted in a significant reduction in inflammatory cytokines. Our study found the idea that the combination of the inhibitor AMD3100 of CXCR4 and the inhibitor L-NIL of iNOS may ameliorate the early brain injury of subarachnoid hemorrhage and could provide a new approach for the future treatment of subarachnoid hemorrhage. However, we did not explain the specific pathways by which L-NIL promotes ferroptosis in M1 microglia, which is also a deficiency of our study. In the future, we will further explore the mechanisms by which L-NIL promotes ferroptosis in M1 microglia.

Abbreviation

SAH Subarachnoid hemorrhage

EBI Early Brain Injury

CXCR4 CXC-chemokine receptor 4

CXCL12 CXC motif chemokine ligand 12

iNOS Inducible nitric oxide synthase

Lip-1 Liproxstatin-1

Elisa Enzyme-Linked Immune Sorbent Assay

FJB Fluoro-Jade B

BBB Blood-brain barrier

CNS Central nervous system

ROS Reactive oxygen species

L-NIL L-N (6)-iminoethyl-lysine

RNS Reactive nitrogen species

Gpx4 Glutathione peroxidase 4

OxyHb Oxyhemoglobin

CSF Cerebrospinal fluid

Lipid-ROS Lipid peroxidation- reactive oxygen species

DAPI 4’, 6-diamidino-2-phenylindol

H2O2 Hydrogen peroxide

DAB 3, 3-diaminobenzidine

LPS Lipopolysaccharides

CCK8 Cell Counting Kit-8

TMB 3, 3, 5, 5-tetramethylbenzidine

MWM Morris Water Maze

STEAP3 Six-transmembrane epithelial antigen of the prostate 3

DMT1 Divalent Metal Transporter 1

Fth Ferritin heavy Chain

Ftl Ferritin light Chain

GSH Glutathione

Cys Cysteine

Ptgs2/COX2 Prostaglandin-endoperoxide synthase 2

Tfr1 Transferrin receptor 1

Tf Transferrin

Declarations

Author contributions

W.Q. and Y.C. contributed equally to this paper. J.Z. and C.L. comprehended the study, provided critical suggestions, contributed to manuscript preparation, oversaw the research program, and wrote the main manuscript.

W.Q., Y.C., and T.R. performed the Western blot, Transwell, Elisa, and immunostaining experiments and analyzed the data.

W.Q., and Y.C. performed the Lipid Peroxidation (Lipid-ROS) Assay, Malondialdehyde (MDA) Content measurement, and analyzed the data.

W.Q., and Y.C., T.R. and W.P. performed the Nissl staining, FJB staining, Perl's staining, the behavioral experiment, and the brain edema test and analyzed the data.

All the authors listed in the manuscript have agreed upon and reviewed the manuscript, and provided feedback.

Funding

This study was supported by the National Nature Science Foundation of China (Nos. 81571121 and 81971163).

Data Availability

All data generated or analyzed during this study are included in this article and its supplementary information files.

Ethics Statement

Our study was approved by the Ethical Committee of Soochow University.

Consent to Participate

Not applicable.

Consent for Publication

Not applicable.

Competing interest

Those authors declare no competing financial interest.

References

1. Macdonald RL (2014) Delayed neurological deterioration after subarachnoid haemorrhage. Nat Rev Neurol 10 (1):44-58. doi:10.1038/nrneurol.2013.246
2. Macdonald RL, Higashida RT, Keller E, Mayer SA, Molyneux A, Raabe A, Vajkoczy P, Wanke I, Bach D, Frey A, Marr A, Roux S, Kassell N (2011) Clazosentan, an endothelin receptor antagonist, in patients with aneurysmal subarachnoid haemorrhage undergoing surgical clipping: a randomised, double-blind, placebo-controlled phase 3 trial (CONSCIOUS-2). The Lancet Neurology 10 (7):618-625. doi:10.1016/s1474-4422(11)70108-9
3. Sehba FA, Hou J, Pluta RM, Zhang JH (2012) The importance of early brain injury after subarachnoid hemorrhage. Prog Neurobiol 97 (1):14-37. doi:10.1016/j.pneurobio.2012.02.003
4. Doll DN, Barr TL, Simpkins JW (2014) Cytokines: their role in stroke and potential use as biomarkers and therapeutic targets. Aging Dis 5 (5):294-306. doi:10.14336/AD.2014.0500294
5. Dheen ST, Kaur C, Ling EA (2007) Microglial activation and its implications in the brain diseases. Curr Med Chem 14 (11):1189-1197. doi:10.2174/092986707780597961
6. Cherry JD, Olschowka JA, O'Banion MK (2014) Neuroinflammation and M2 microglia: the good, the bad, and the inflamed. J Neuroinflammation 11:98. doi:10.1186/1742-2094-11-98
7. Perego C, Fumagalli S, De Simoni MG (2011) Temporal pattern of expression and colocalization of microglia/macrophage phenotype markers following brain ischemic injury in mice. J Neuroinflammation 8:174. doi:10.1186/1742-2094-8-174
8. Kobayashi K, Imagama S, Ohgomori T, Hirano K, Uchimura K, Sakamoto K, Hirakawa A, Takeuchi H, Suzumura A, Ishiguro N, Kadomatsu K (2013) Minocycline selectively inhibits M1 polarization of microglia. Cell Death Dis 4:e525. doi:10.1038/cddis.2013.54

9. Taylor RA, Sansing LH (2013) Microglial responses after ischemic stroke and intracerebral hemorrhage. Clin Dev Immunol 2013:746068. doi:10.1155/2013/746068
10. Ponomarev ED, Maresz K, Tan Y, Dittel BN (2007) CNS-derived interleukin-4 is essential for the regulation of autoimmune inflammation and induces a state of alternative activation in microglial cells. J Neurosci 27 (40):10714-10721. doi:10.1523/JNEUROSCI.1922-07.2007
11. Xie Y, Peng J, Pang J, Guo K, Zhang L, Yin S, Zhou J, Gu L, Tu T, Mu Q, Liao Y, Zhang X, Chen L, Jiang Y (2020) Biglycan regulates neuroinflammation by promoting M1 microglial activation in early brain injury after experimental subarachnoid hemorrhage. J Neurochem 152 (3):368-380. doi:10.1111/jnc.14926
12. Mennicken F, Maki R, de Souza EB, Quirion R (1999) Chemokines and chemokine receptors in the CNS: a possible role in neuroinflammation and patterning. Trends Pharmacol Sci 20 (2):73-78. doi:10.1016/s0165-6147(99)01308-5
13. Ohtani Y, Minami M, Kawaguchi N, Nishiyori A, Yamamoto J, Takami S, Satoh M (1998) Expression of stromal cell-derived factor-1 and CXCR4 chemokine receptor mRNAs in cultured rat glial and neuronal cells. Neurosci Lett 249 (2-3):163-166. doi:10.1016/s0304-3940(98)00425-x
14. Tanabe S, Heesen M, Yoshizawa I, Berman MA, Luo Y, Bleul CC, Springer TA, Okuda K, Gerard N, Dorf ME (1997) Functional expression of the CXC-chemokine receptor-4/fusin on mouse microglial cells and astrocytes. J Immunol 159 (2):905-911
15. Lipfert J, Odemis V, Wagner DC, Boltze J, Engele J (2013) CXCR4 and CXCR7 form a functional receptor unit for SDF-1/CXCL12 in primary rodent microglia. Neuropathol Appl Neurobiol 39 (6):667-680. doi:10.1111/nan.12015
16. Dixon SJ, Lemberg KM, Lamprecht MR, Skouta R, Zaitsev EM, Gleason CE, Patel DN, Bauer AJ, Cantley AM, Yang WS, Morrison B, 3rd, Stockwell BR (2012) Ferroptosis: an iron-dependent form of nonapoptotic cell death. Cell 149 (5):1060-1072. doi:10.1016/j.cell.2012.03.042
17. Stockwell BR, Friedmann Angeli JP, Bayir H, Bush AI, Conrad M, Dixon SJ, Fulda S, Gascon S, Hatzios SK, Kagan VE, Noel K, Jiang X, Linkermann A, Murphy ME, Overholtzer M, Oyagi A, Pagnussat GC, Park J, Ran Q, Rosenfeld CS, Salnikow K, Tang D, Torti FM, Torti SV, Toyokuni S, Woerpel KA, Zhang DD (2017) Ferroptosis: A Regulated Cell Death Nexus Linking Metabolism, Redox Biology, and Disease. Cell 171 (2):273-285. doi:10.1016/j.cell.2017.09.021
18. Friedmann Angeli JP, Schneider M, Proneth B, Tyurina YY, Tyurin VA, Hammond VJ, Herbach N, Aichler M, Walch A, Eggenhofer E, Basavarajappa D, Radmark O, Kobayashi S, Seibt T, Beck H, Neff F, Esposito I, Wanke R, Forster H, Yefremova O, Heinrichmeyer M, Bornkamm GW, Geissler EK, Thomas SB, Stockwell BR, O'Donnell VB, Kagan VE, Schick JA, Conrad M (2014) Inactivation of the ferroptosis regulator Gpx4 triggers acute renal failure in mice. Nat Cell Biol 16 (12):1180-1191. doi:10.1038/ncb3064
19. Gugiu BG, Mesaros CA, Sun M, Gu X, Crabb JW, Salomon RG (2006) Identification of oxidatively truncated ethanolamine phospholipids in retina and their generation from polyunsaturated phosphatidylethanolamines. Chem Res Toxicol 19 (2):262-271. doi:10.1021/tx050247f

20. Stoyanovsky DA, Tyurina YY, Shrivastava I, Bahar I, Tyurin VA, Protchenko O, Jadhav S, Bolevich SB, Kozlov AV, Vladimirov YA, Shvedova AA, Philpott CC, Bayir H, Kagan VE (2019) Iron catalysis of lipid peroxidation in ferroptosis: Regulated enzymatic or random free radical reaction? Free Radic Biol Med 133:153-161. doi:10.1016/j.freeradbiomed.2018.09.008
21. Hoff HF, O'Neil J, Wu Z, Hoppe G, Salomon RL (2003) Phospholipid hydroxyalkenals: biological and chemical properties of specific oxidized lipids present in atherosclerotic lesions. Arterioscler Thromb Vasc Biol 23 (2):275-282. doi:10.1161/01.atv.0000051407.42536.73
22. Pizzimenti S, Ciamporcero E, Daga M, Pettazzoni P, Arcaro A, Cetrangolo G, Minelli R, Dianzani C, Lepore A, Gentile F, Barrera G (2013) Interaction of aldehydes derived from lipid peroxidation and membrane proteins. Front Physiol 4:242. doi:10.3389/fphys.2013.00242
23. Kapralov AA, Yang Q, Dar HH, Tyurina YY, Anthonymuthu TS, Kim R, St Croix CM, Mikulska-Ruminska K, Liu B, Shrivastava IH, Tyurin VA, Ting HC, Wu YL, Gao Y, Shurin GV, Artyukhova MA, Ponomareva LA, Timashev PS, Domingues RM, Stoyanovsky DA, Greenberger JS, Mallampalli RK, Bahar I, Gabrilovich DI, Bayir H, Kagan VE (2020) Redox lipid reprogramming commands susceptibility of macrophages and microglia to ferroptotic death. Nat Chem Biol 16 (3):278-290. doi:10.1038/s41589-019-0462-8
24. Luo Y, Yin X, Shi S, Ren X, Zhang H, Wang Z, Cao Y, Tang M, Xiao B, Zhang M (2019) Non-destructive 3D Microtomography of Cerebral Angioarchitecture Changes Following Ischemic Stroke in Rats Using Synchrotron Radiation. Front Neuroanat 13:5. doi:10.3389/fnana.2019.00005
25. Devine SM, Flomenberg N, Vesole DH, Liesveld J, Weisdorf D, Badel K, Calandra G, DiPersio JF (2004) Rapid mobilization of CD34+ cells following administration of the CXCR4 antagonist AMD3100 to patients with multiple myeloma and non-Hodgkin's lymphoma. J Clin Oncol 22 (6):1095-1102. doi:10.1200/JCO.2004.07.131
26. Hendrix CW, Flexner C, MacFarland RT, Giandomenico C, Fuchs EJ, Redpath E, Bridger G, Henson GW (2000) Pharmacokinetics and safety of AMD-3100, a novel antagonist of the CXCR-4 chemokine receptor, in human volunteers. Antimicrob Agents Chemother 44 (6):1667-1673. doi:10.1128/AAC.44.6.1667-1673.2000
27. Liles WC, Broxmeyer HE, Rodger E, Wood B, Hubel K, Cooper S, Hangoc G, Bridger GJ, Henson GW, Calandra G, Dale DC (2003) Mobilization of hematopoietic progenitor cells in healthy volunteers by AMD3100, a CXCR4 antagonist. Blood 102 (8):2728-2730. doi:10.1182/blood-2003-02-0663
28. Mao L, Huang M, Chen SC, Li YN, Xia YP, He QW, Wang MD, Huang Y, Zheng L, Hu B (2014) Endogenous endothelial progenitor cells participate in neovascularization via CXCR4/SDF-1 axis and improve outcome after stroke. CNS Neurosci Ther 20 (5):460-468. doi:10.1111/cns.12238
29. Zhang JY, Wang Y, Milton MN, Kraus L, Breau AP, Paulson SK (2004) Disposition and pharmacokinetics of L-N6-(1-iminoethyl)lysine-5-tetrazole-amide, a selective iNOS inhibitor, in rats. J Pharm Sci 93 (5):1229-1240. doi:10.1002/jps.20048
30. Qu XF, Liang TY, Wu DG, Lai NS, Deng RM, Ma C, Li X, Li HY, Liu YZ, Shen HT, Chen G (2021) Acyl-CoA synthetase long chain family member 4 plays detrimental role in early brain injury after

subarachnoid hemorrhage in rats by inducing ferroptosis. CNS Neurosci Ther 27 (4):449-463. doi:10.1111/cns.13548

31. Xie BS, Wang YQ, Lin Y, Mao Q, Feng JF, Gao GY, Jiang JY (2019) Inhibition of ferroptosis attenuates tissue damage and improves long-term outcomes after traumatic brain injury in mice. CNS Neurosci Ther 25 (4):465-475. doi:10.1111/cns.13069
32. Liu HC, Zheng MH, Du YL, Wang L, Kuang F, Qin HY, Zhang BF, Han H (2012) N9 microglial cells polarized by LPS and IL4 show differential responses to secondary environmental stimuli. Cell Immunol 278 (1-2):84-90. doi:10.1016/j.cellimm.2012.06.001
33. Li Y, Xia Y, Wang Y, Mao L, Gao Y, He Q, Huang M, Chen S, Hu B (2013) Sonic hedgehog (Shh) regulates the expression of angiogenic growth factors in oxygen-glucose-deprived astrocytes by mediating the nuclear receptor NR2F2. Mol Neurobiol 47 (3):967-975. doi:10.1007/s12035-013-8395-9
34. Alfieri JA, Pino NS, Igaz LM (2014) Reversible behavioral phenotypes in a conditional mouse model of TDP-43 proteinopathies. J Neurosci 34 (46):15244-15259. doi:10.1523/JNEUROSCI.1918-14.2014
35. Luo CL, Li BX, Li QQ, Chen XP, Sun YX, Bao HJ, Dai DK, Shen YW, Xu HF, Ni H, Wan L, Qin ZH, Tao LY, Zhao ZQ (2011) Autophagy is involved in traumatic brain injury-induced cell death and contributes to functional outcome deficits in mice. Neuroscience 184:54-63. doi:10.1016/j.neuroscience.2011.03.021
36. Guo F, Hua Y, Wang J, Keep RF, Xi G (2012) Inhibition of carbonic anhydrase reduces brain injury after intracerebral hemorrhage. Transl Stroke Res 3 (1):130-137. doi:10.1007/s12975-011-0106-0
37. He Z, Ostrowski RP, Sun X, Ma Q, Huang B, Zhan Y, Zhang JH (2012) CHOP silencing reduces acute brain injury in the rat model of subarachnoid hemorrhage. Stroke 43 (2):484-490. doi:10.1161/STROKEAHA.111.626432
38. Garcia JH, Wagner S, Liu KF, Hu XJ (1995) Neurological deficit and extent of neuronal necrosis attributable to middle cerebral artery occlusion in rats. Statistical validation. Stroke 26 (4):627-634; discussion 635. doi:10.1161/01.str.26.4.627
39. Ma Z, Zhang Z, Bai F, Jiang T, Yan C, Wang Q (2019) Electroacupuncture Pretreatment Alleviates Cerebral Ischemic Injury Through alpha7 Nicotinic Acetylcholine Receptor-Mediated Phenotypic Conversion of Microglia. Front Cell Neurosci 13:537. doi:10.3389/fncel.2019.00537
40. Zhao R, Ying M, Gu S, Yin W, Li Y, Yuan H, Fang S, Li M (2019) Cysteinyl Leukotriene Receptor 2 is Involved in Inflammation and Neuronal Damage by Mediating Microglia M1/M2 Polarization through NF-kappaB Pathway. Neuroscience 422:99-118. doi:10.1016/j.neuroscience.2019.10.048
41. Kigerl KA, Gensel JC, Ankeny DP, Alexander JK, Donnelly DJ, Popovich PG (2009) Identification of two distinct macrophage subsets with divergent effects causing either neurotoxicity or regeneration in the injured mouse spinal cord. J Neurosci 29 (43):13435-13444. doi:10.1523/JNEUROSCI.3257-09.2009
42. Quirie A, Demougeot C, Bertrand N, Mossiat C, Garnier P, Marie C, Prigent-Tessier A (2013) Effect of stroke on arginase expression and localization in the rat brain. Eur J Neurosci 37 (7):1193-1202.

doi:10.1111/ejn.12111

43. Hill WD, Hess DC, Martin-Studdard A, Carothers JJ, Zheng J, Hale D, Maeda M, Fagan SC, Carroll JE, Conway SJ (2004) SDF-1 (CXCL12) is upregulated in the ischemic penumbra following stroke: association with bone marrow cell homing to injury. J Neuropathol Exp Neurol 63 (1):84-96. doi:10.1093/jnen/63.1.84
44. Calderon TM, Eugenin EA, Lopez L, Kumar SS, Hesselgesser J, Raine CS, Berman JW (2006) A role for CXCL12 (SDF-1alpha) in the pathogenesis of multiple sclerosis: regulation of CXCL12 expression in astrocytes by soluble myelin basic protein. J Neuroimmunol 177 (1-2):27-39. doi:10.1016/j.jneuroim.2006.05.003
45. Krumbholz M, Theil D, Cepok S, Hemmer B, Kivisakk P, Ransohoff RM, Hofbauer M, Farina C, Derfuss T, Hartle C, Newcombe J, Hohlfeld R, Meinl E (2006) Chemokines in multiple sclerosis: CXCL12 and CXCL13 up-regulation is differentially linked to CNS immune cell recruitment. Brain 129 (Pt 1):200-211. doi:10.1093/brain/awh680
46. McCandless EE, Piccio L, Woerner BM, Schmidt RE, Rubin JB, Cross AH, Klein RS (2008) Pathological expression of CXCL12 at the blood-brain barrier correlates with severity of multiple sclerosis. Am J Pathol 172 (3):799-808. doi:10.2353/ajpath.2008.070918
47. Huang M, Wan Y, Mao L, He QW, Xia YP, Li M, Li YN, Jin HJ, Hu B (2017) Inhibiting the Migration of M1 Microglia at Hyperacute Period Could Improve Outcome of tMCAO Rats. CNS Neurosci Ther 23 (3):222-232. doi:10.1111/cns.12665
48. Chen C, Chen J, Wang Y, Liu Z, Wu Y (2020) Ferroptosis drives photoreceptor degeneration in mice with defects in all-trans-retinal clearance. J Biol Chem. doi:10.1074/jbc.RA120.015779
49. Chen S, Ma Q, Krafft PR, Hu Q, Rolland W, 2nd, Sherchan P, Zhang J, Tang J, Zhang JH (2013) P2X7R/cryopyrin inflammasome axis inhibition reduces neuroinflammation after SAH. Neurobiol Dis 58:296-307. doi:10.1016/j.nbd.2013.06.011
50. He Y, Xu L, Li B, Guo ZN, Hu Q, Guo Z, Tang J, Chen Y, Zhang Y, Tang J, Zhang JH (2015) Macrophage-Inducible C-Type Lectin/Spleen Tyrosine Kinase Signaling Pathway Contributes to Neuroinflammation After Subarachnoid Hemorrhage in Rats. Stroke 46 (8):2277-2286. doi:10.1161/STROKEAHA.115.010088
51. Pradilla G, Chaichana KL, Hoang S, Huang J, Tamargo RJ (2010) Inflammation and cerebral vasospasm after subarachnoid hemorrhage. Neurosurg Clin N Am 21 (2):365-379. doi:10.1016/j.nec.2009.10.008
52. Zheng VZ, Wong GKC (2017) Neuroinflammation responses after subarachnoid hemorrhage: A review. J Clin Neurosci 42:7-11. doi:10.1016/j.jocn.2017.02.001
53. Gregersen R, Lambertsen K, Finsen B (2000) Microglia and macrophages are the major source of tumor necrosis factor in permanent middle cerebral artery occlusion in mice. J Cereb Blood Flow Metab 20 (1):53-65. doi:10.1097/00004647-200001000-00009
54. Fumagalli S, Perego C, Pischiutta F, Zanier ER, De Simoni MG (2015) The ischemic environment drives microglia and macrophage function. Front Neurol 6:81. doi:10.3389/fneur.2015.00081

55. Denes A, Vidyasagar R, Feng J, Narvainen J, McColl BW, Kauppinen RA, Allan SM (2007) Proliferating resident microglia after focal cerebral ischaemia in mice. J Cereb Blood Flow Metab 27 (12):1941-1953. doi:10.1038/sj.jcbfm.9600495
56. Schilling M, Besselmann M, Leonhard C, Mueller M, Ringelstein EB, Kiefer R (2003) Microglial activation precedes and predominates over macrophage infiltration in transient focal cerebral ischemia: a study in green fluorescent protein transgenic bone marrow chimeric mice. Experimental Neurology 183 (1):25-33. doi:10.1016/s0014-4886(03)00082-7
57. Schilling M, Besselmann M, Muller M, Strecker JK, Ringelstein EB, Kiefer R (2005) Predominant phagocytic activity of resident microglia over hematogenous macrophages following transient focal cerebral ischemia: an investigation using green fluorescent protein transgenic bone marrow chimeric mice. Exp Neurol 196 (2):290-297. doi:10.1016/j.expneurol.2005.08.004
58. Zhao S, Qu H, Zhao Y, Xiao T, Zhao M, Li Y, Jolkkonen J, Cao Y, Zhao C (2015) CXCR4 antagonist AMD3100 reverses the neurogenesis and behavioral recovery promoted by forced limb-use in stroke rats. Restor Neurol Neurosci 33 (6):809-821. doi:10.3233/RNN-150515
59. Ingold I, Berndt C, Schmitt S, Doll S, Poschmann G, Buday K, Roveri A, Peng X, Porto Freitas F, Seibt T, Mehr L, Aichler M, Walch A, Lamp D, Jastroch M, Miyamoto S, Wurst W, Ursini F, Arner ESJ, Fradejas-Villar N, Schweizer U, Zischka H, Friedmann Angeli JP, Conrad M (2018) Selenium Utilization by GPX4 Is Required to Prevent Hydroperoxide-Induced Ferroptosis. Cell 172 (3):409-422 e421. doi:10.1016/j.cell.2017.11.048
60. Bridges RJ, Natale NR, Patel SA (2012) System xc(-) cystine/glutamate antiporter: an update on molecular pharmacology and roles within the CNS. Br J Pharmacol 165 (1):20-34. doi:10.1111/j.1476-5381.2011.01480.x
61. Zhang Z, Guo M, Li Y, Shen M, Kong D, Shao J, Ding H, Tan S, Chen A, Zhang F, Zheng S (2020) RNA-binding protein ZFP36/TTP protects against ferroptosis by regulating autophagy signaling pathway in hepatic stellate cells. Autophagy 16 (8):1482-1505. doi:10.1080/15548627.2019.1687985
62. Piastra M, Caresta E, Massimi L, Picconi E, Luca E, Morena TC, Conti G, Eaton S (2020) Lipid Peroxidation and Antioxidant Consumption as Early Markers of Neurosurgery-Related Brain Injury in Children. Neurocrit Care 33 (1):124-131. doi:10.1007/s12028-019-00870-w
63. Partyka A, Lukaszewicz E, Nizanski W, Twardon J (2011) Detection of lipid peroxidation in frozen-thawed avian spermatozoa using C(11)-BODIPY(581/591). Theriogenology 75 (9):1623-1629. doi:10.1016/j.theriogenology.2011.01.002

Figures

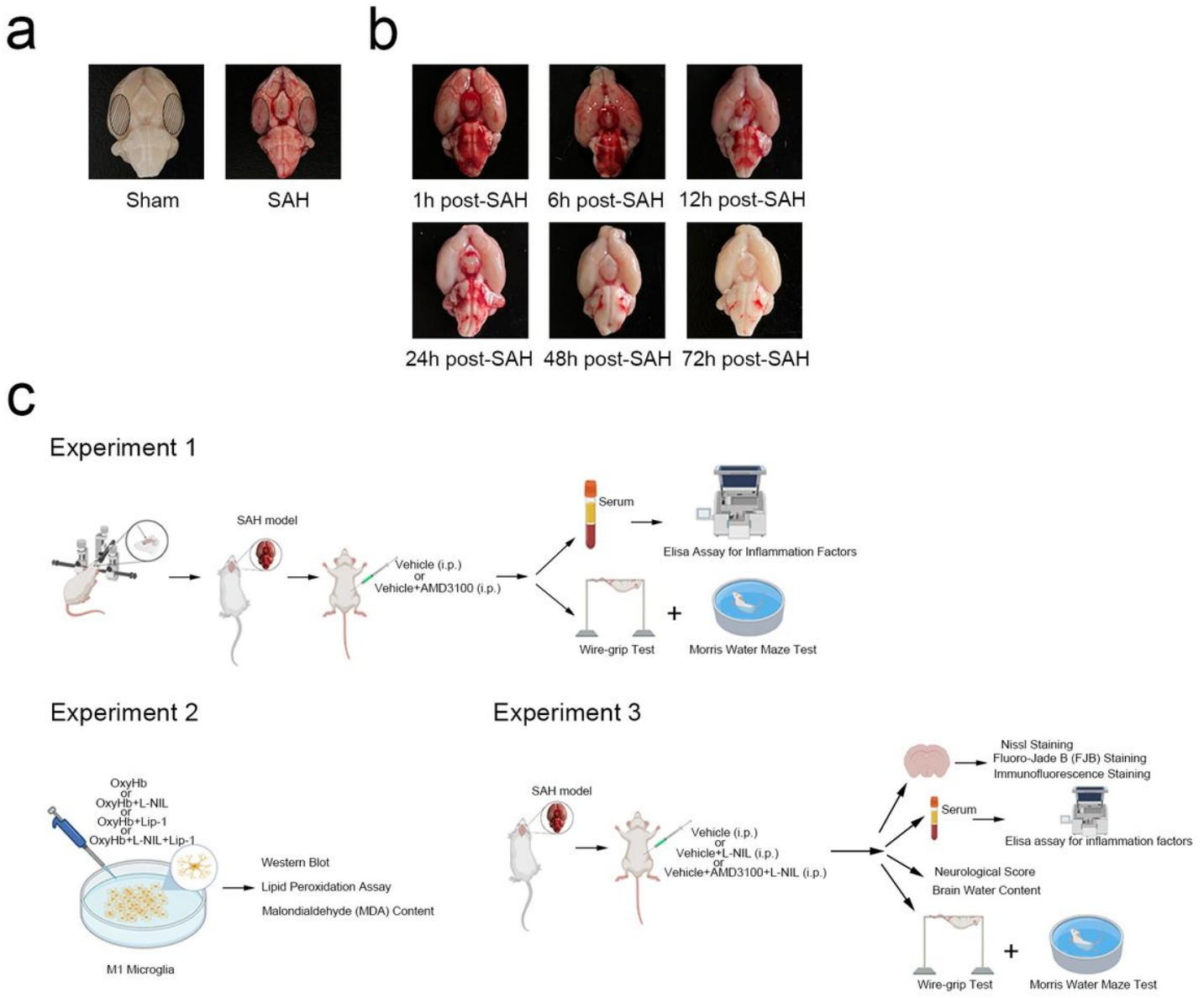

Figure 1

Brain tissue of rats at the indicated time points after subarachnoid hemorrhage modeling, and the frame of experimental design. (a) Brain tissues were collected from sham and SAH-model group rat's temporal floor, which is the shaded area in the figure. (b) Rats were sacrificed at different time points after the SAH model:1 h,6 h,12 h,24 h,48 h,72 h. The brain tissue shown here is post-perfusion brain tissue from a rat at the indicated time points after SAH. (c) A series of experiments to assess the effect of AMD3100 and L-NIL on the prognosis of SAH rats.

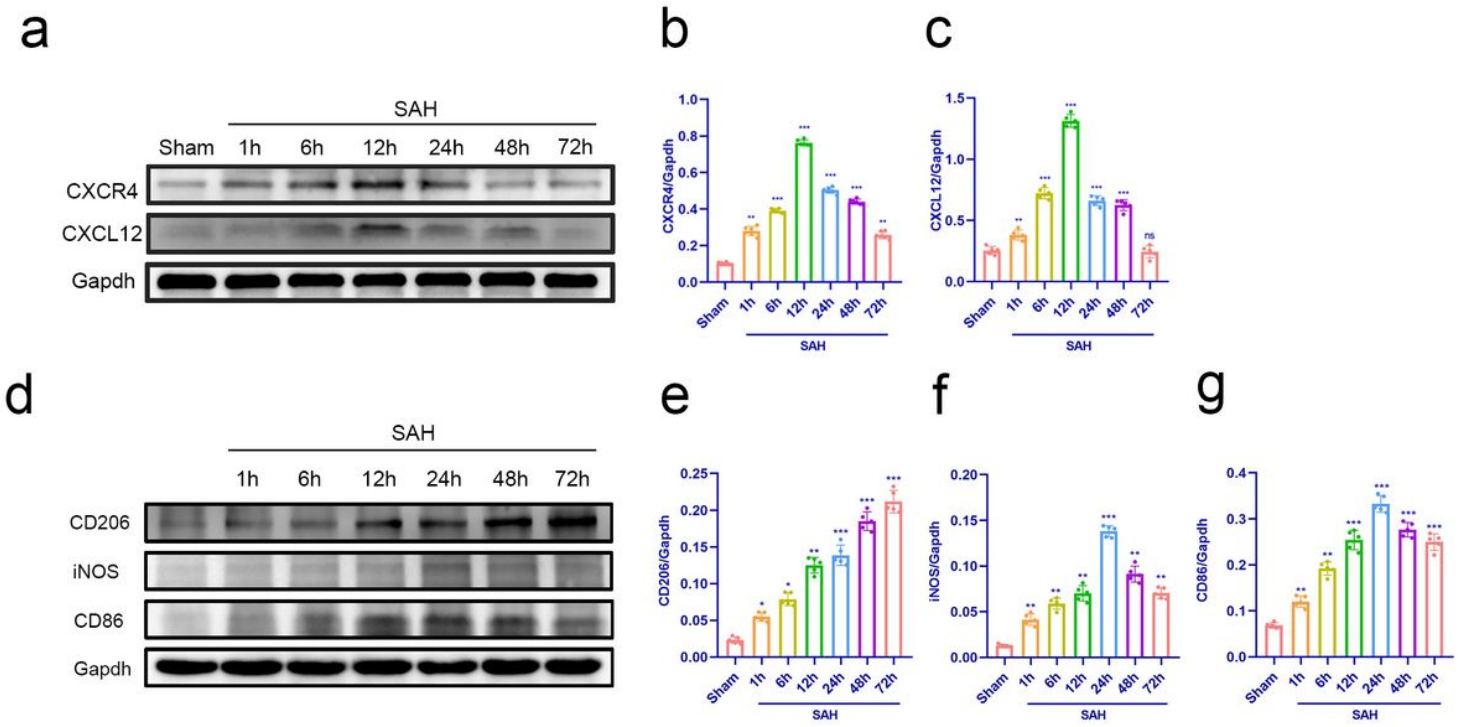

Figure 2

The expression level of CXCR4, CXCL12, CD205, iNOS, and CD86 at the indicated time points after the SAH model. (a)The expression of CXCR4 and CXCL12 in temporal-floor brain tissue was detected by western blot at 1h, 6h, 12h, 24h, 48h, and 72h after the SAH model; each group set contained 5 samples (n=5). Data are expressed as the ratio of CXCR4/Gapdh (b) and CXCL12/Gapdh (c). (d)The expression of CD206, iNOS, and CD86 in temporal-floor brain tissue was detected by western blot at 1h, 6h, 12h, 24h, 48h, and 72h after the SAH model; each group set contained 5 samples (n=5). Data are expressed as the ratio of CD206/Gapdh (e), iNOS/Gapdh (f), and CD86/Gapdh (g). *P < 0.05, **P < 0.01, and ***P <0.001 versus Sham group;

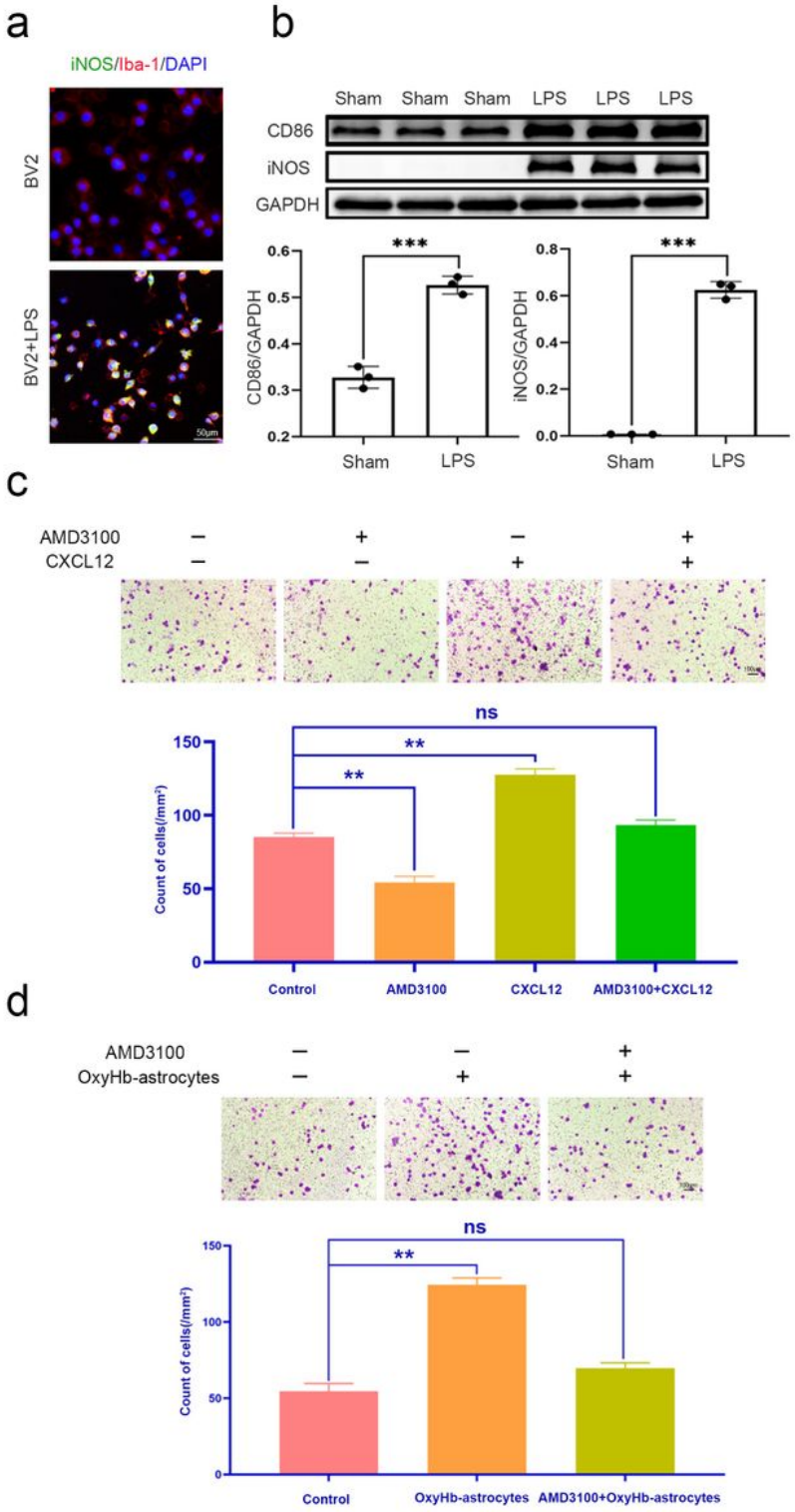

Figure 3

CXCR4/CXCL12 was the critical pathway of the migration of M1 Microglia in vitro. (a) Immunofluorescent double staining was performed for BV2 microglia: iNOS (green) and Iba-1 (red) in the presence or absence of LPS. The nuclei were stained with DAPI. (b)Western blot was performed to detect the expression of M1-associated biomarkers (CD86, iNOS) in BV2 microglia stimulated by LPS, at least in triplicate(n=3). Data are expressed as the ratio of CD86/Gapdh and iNOS/Gapdh. (c)The image showed the transwell system

was used to show the migration of M1 microglia affected by AMD3100 under the condition with or without CXCL12 (upper panel). Quantification of migrated M1 microglia number per square millimeter on the opposite surface (lower panel; **P < 0.001; n=3). (d)The image showed the transwell system was used to show migration of M1 microglia affected by AMD3100 under the condition with or without OxyHb induced astrocytes (upper panel). Quantification of migrated M1 microglia number per square millimeter on the opposite surface (lower panel; **P < 0.001; n=3).

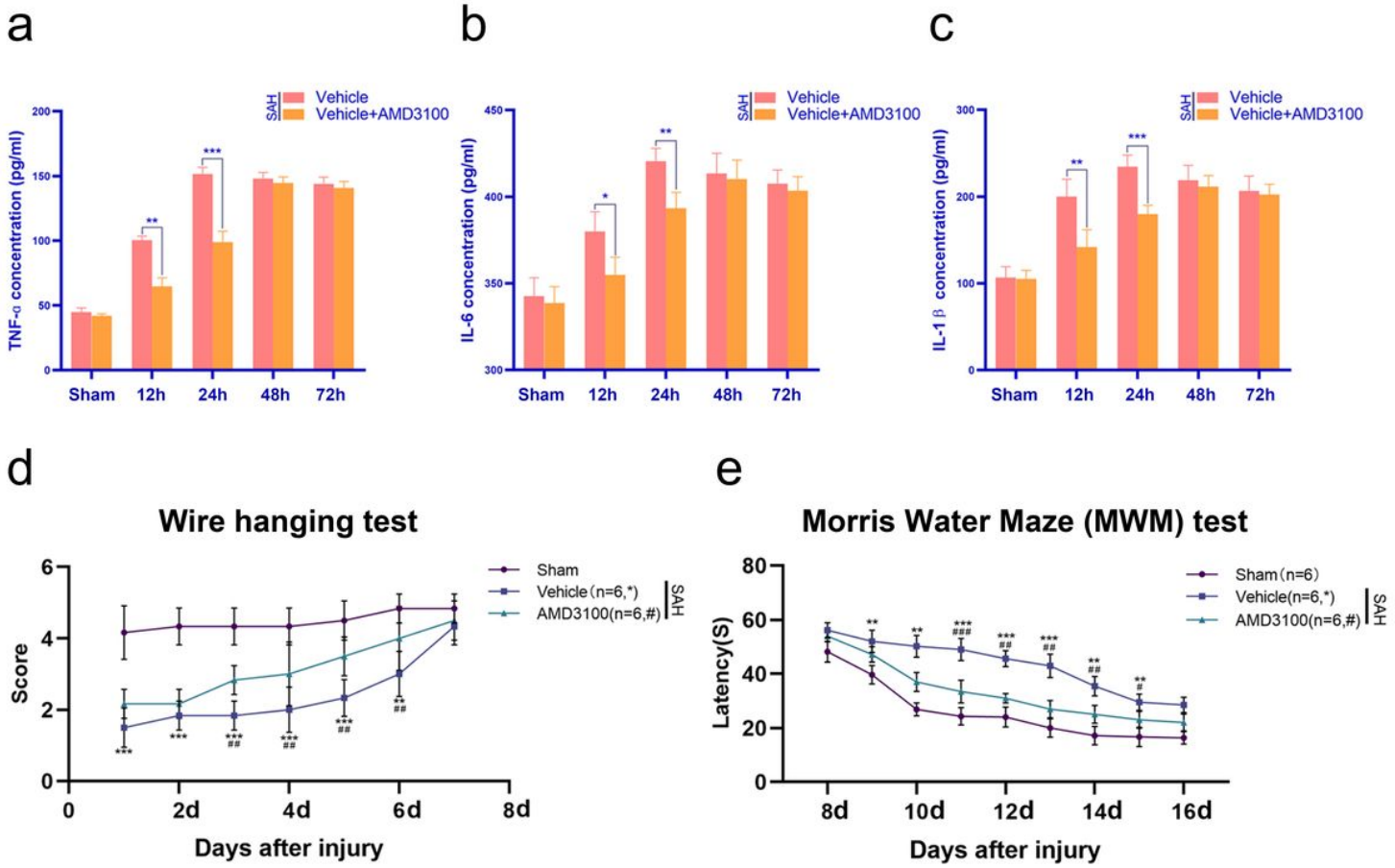

Figure 4

Disturbing CXCL12/CXCR4 pathway in the first 24h after SAH could inhibit the inflammation responses and improve the outcome. Serum was collected from the SAH rats at specific time after model: 12h, 24h, 48h, and 72h. The expression of inflammation factors at specific time points after AMD3100 or vehicle treatment was measured. The activity levels of the inflammatory cytokines :(a) TNF-α, (b) IL-6, (c) IL-1β were measured using ELISA kits. *P < 0.05, **P < 0.01, ***P < 0.001 versus Vehicle, each group set contained 6 samples. The SAH rats was used to performed wire-grip test and morris water maze test on the condition with and without AMD3100 or vehicle treatment. (d) The score of each group in wire-grip test within 7days after SAH model, **P < 0.01 and ***P < 0.001 versus Sham group, #P < 0.05, ##P < 0.01and ###P < 0.001 versus Vehicle, each group set contained 6 samples (n=6). (e) The latency of each group in morris water maze test after SAH model within 8-16 days. **P < 0.01 and ***P < 0.001 versus Sham group, #P < 0.05, ##P < 0.01and ###P < 0.001 versus Vehicle, each group set contained 6 samples (n=6).

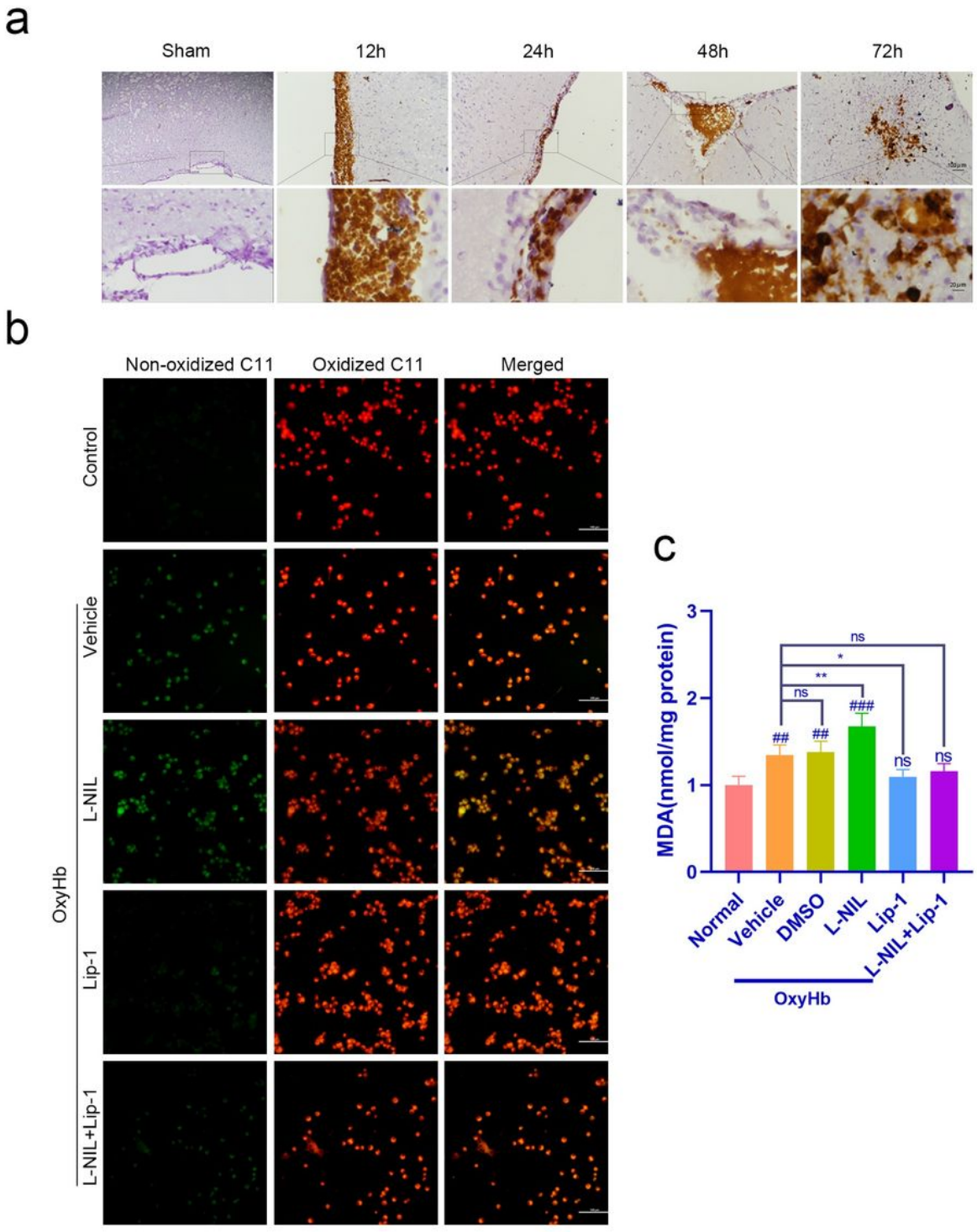

Figure 5

Perls' Prussian blue staining of rats' brain slices and lipid peroxidation assay of M1 microglia. (a) Perls' Prussian blue staining was performed with the brain sections at 1h,6h,12h,24h,48h,72h after SAH; the scale bars represent 100 μm and 20 μm, respectively. (b) BODIRY 581/591 C11 was used to assess the effect of OxyHb, L-NIL, and Lip-1 on the lipid ROS level of M1 microglia. The picture of non-oxidized C11, oxidized C11, and merge was captured. The scale bars represent 100 μm. (c) The MDA was measured in

OxyHb-induced M1 microglia, which was treated with L-NIL and Lip-1. *P < 0.05 and **P < 0.01 versus Normal group, ##P < 0.01and ###P < 0.001 versus Vehicle, each group set contained 5 samples (n=5).

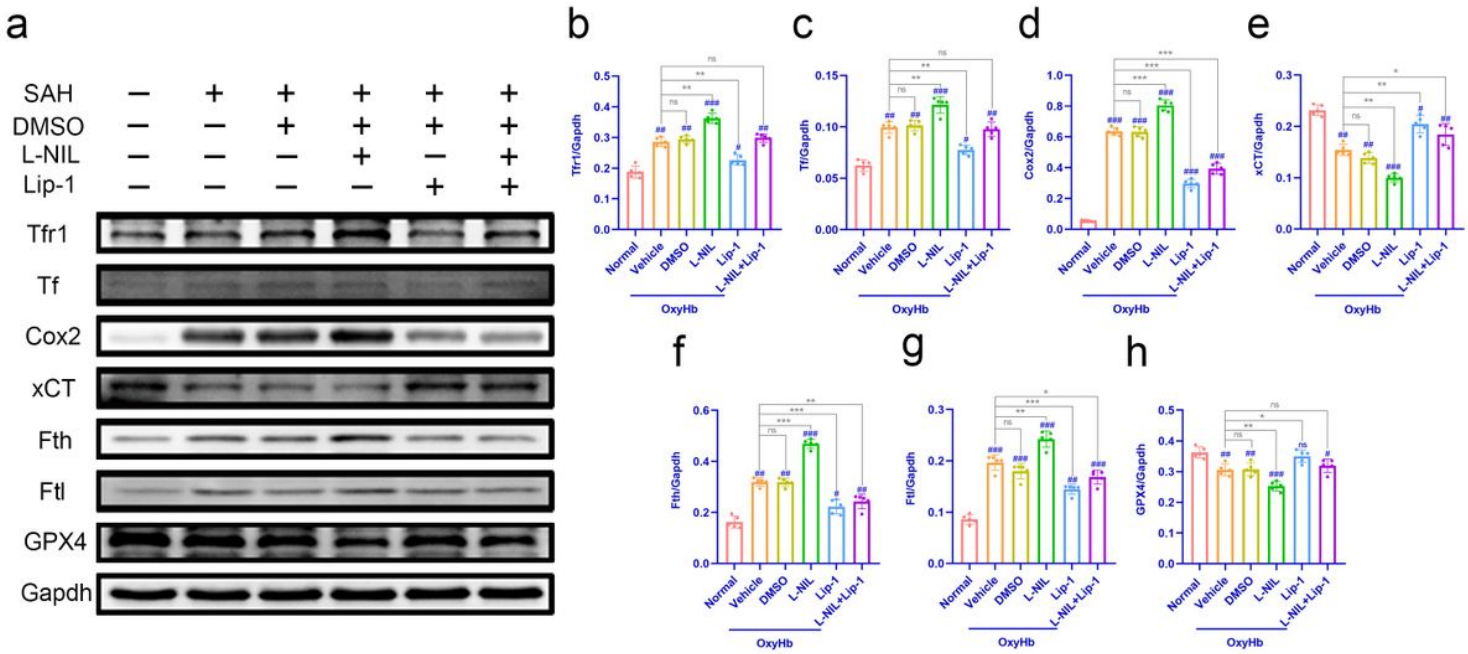

Figure 6

The effect of L-NIL treatment on ferroptosis of M1 microglia. BV-2 microglia were collected 6h after OxyHb-induced. The cells of Normal, OxyHb, OxyHb+DMSO, OxyHb+DMSO+L-NIL, OxyHb+DMSO+Lip-1, OxyHb+DMSO+L-NIL+Lip-1 groups were collected. (a)Western blot for Tfr1, Tf, Cox2, xCT, Fth, Ftl, and GPX4 was performed; each group set contained 5 samples (n=5). The expression level of Tfr1(b), Tf(c), Cox2(d), xCT(e), Fth(f), Ftl(g), and GPX4(h) in BV-2 microglia was detected under the condition with or without L-NIL or Lip-1 treatment. Data are expressed as the ratio of Tfr1/Gapdh, Tf/Gapdh, Cox2/Gapdh, xCT/Gapdh, Fth/Gapdh, Ftl/Gapdh, and GPX4/Gapdh. #P < 0.05, ##P < 0.01, and ###P <0.001 versus Normal group; *P < 0.05, **P < 0.01, and ***P <0.001 versus Vehicle group.

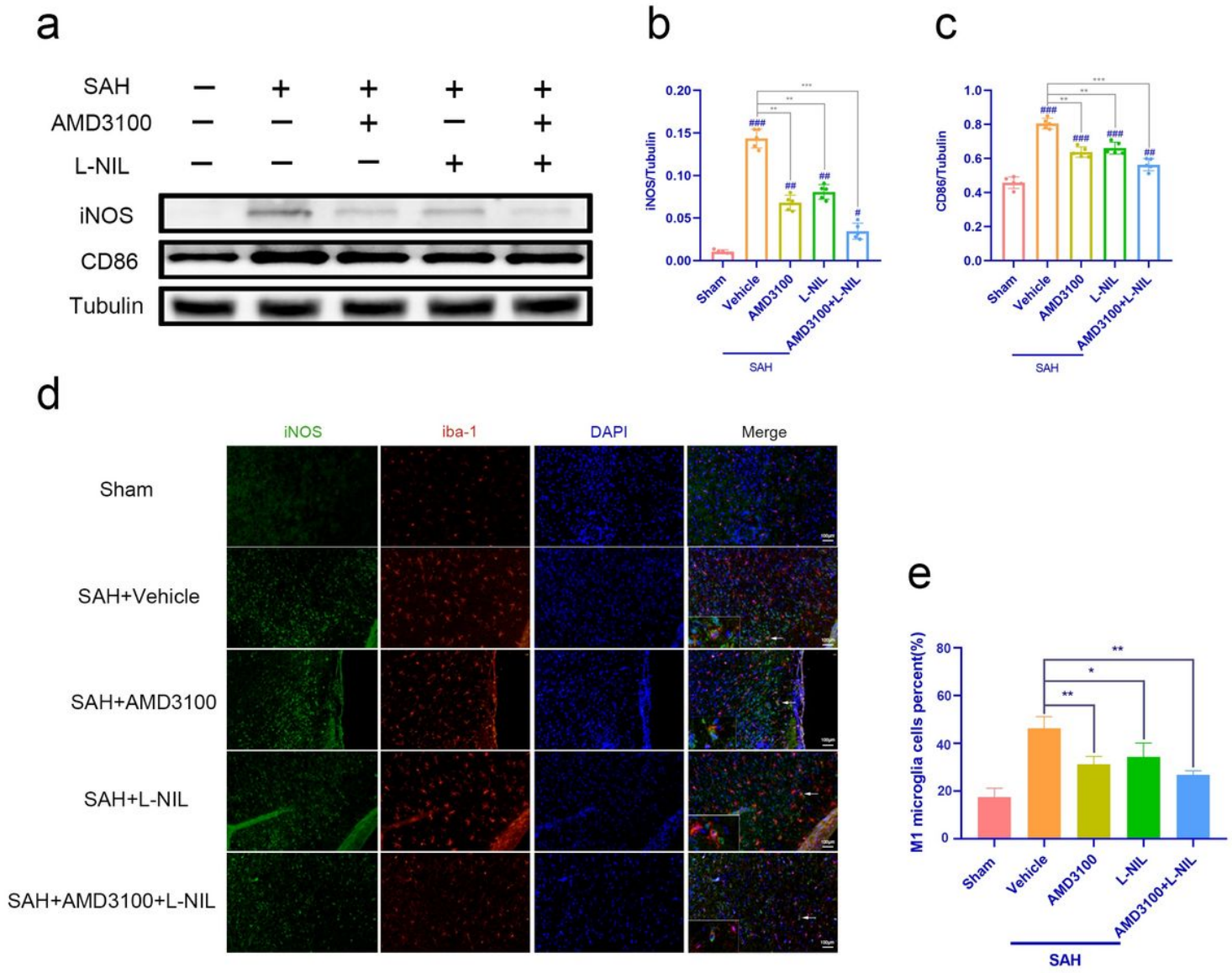

Figure 7

Quantity of M1 microglia was decreased by the treatment of AMD3100 and L-NIL. Rats were sacrificed 1 day after SAH. (a)The brain of Sham, SAH+Vehicle, SAH+AMD3100, SAH+L-NIL, and SAH+AMD3100+L-NIL groups were obtained. Western blot for iNOS and CD86 in temporal-floor brain tissue was performed; each group set contained 5 samples (n=5). The expression level of iNOS in temporal-floor brain tissue was detected under the condition with or without treatment of AMD3100 or L-NIL. Data are expressed as the ratio of iNOS/Tubulin (b). The expression level of CD86 in temporal-floor brain tissue was detected under the condition with or without treatment of AMD3100 or L-NIL. Data are expressed as the ratio of CD86/Tubulin (c). #P < 0.05, ##P < 0.01, and ###P <0.001 versus Sham group; *P < 0.05 and **P < 0.01 versus Vehicle group. Rats were sacrificed 24h after the SAH model. The brain slices of Sham, SAH+Vehicle, SAH+AMD3100, SAH+L-NIL, and SAH+AMD3100+L-NIL groups were obtained. (d) Immunofluorescent double staining was performed for the brain slices: iNOS (green) and Iba-1 (red) in the presence or absence of AMD3100 or L-NIL. The nuclei were stained with DAPI. Double positive cells

indicated by arrows are shown at higher magnification in the left-bottom panels. (e) Data were expressed as the percent of Merge/Iba-1; *P < 0.05 and **P < 0.01 versus Vehicle group; the scale bars represent 100 μm.

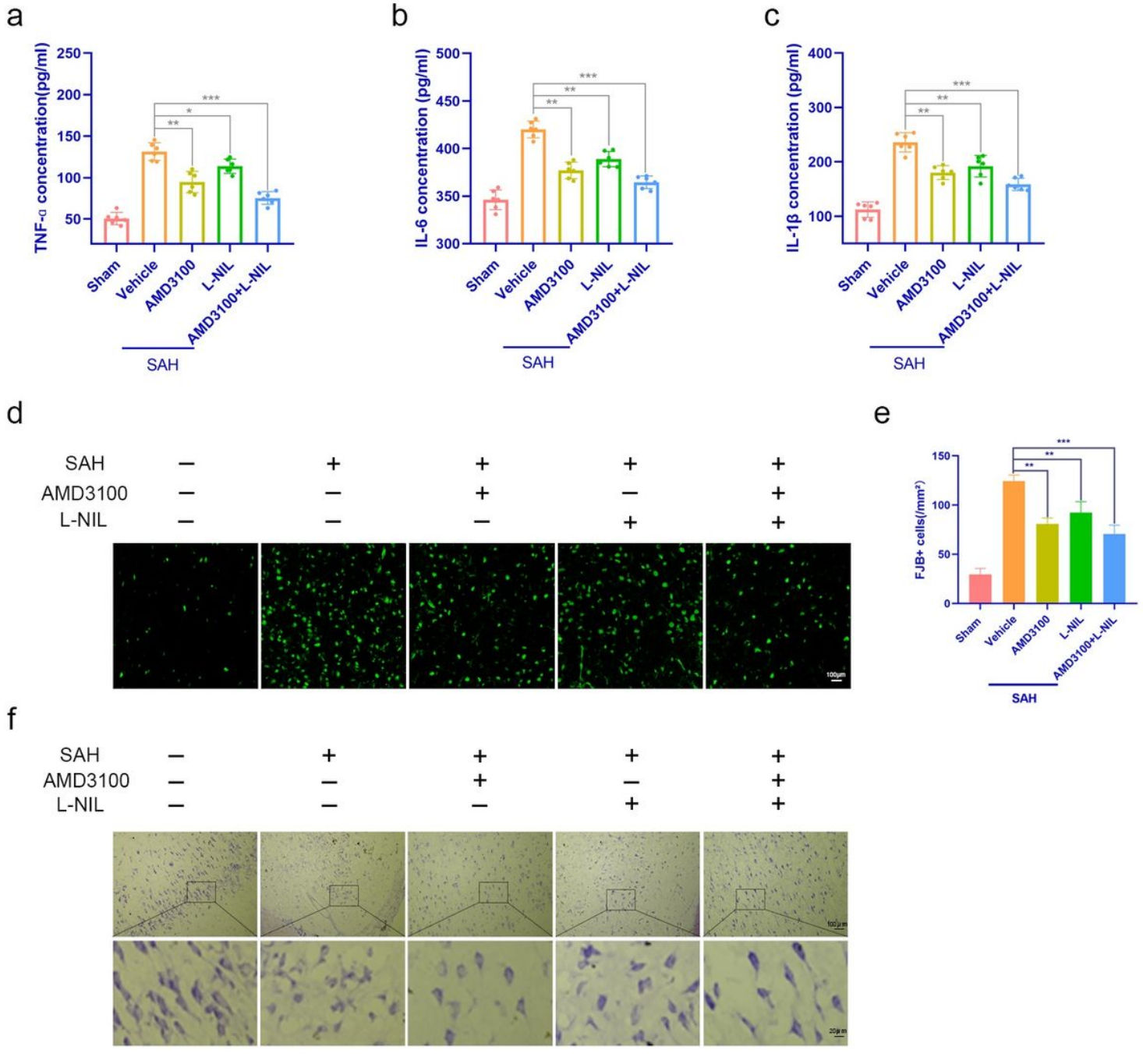

Figure 8

Both AMD3100 and L-NIL alleviated inflammation and rescued the neuronal damage after SAH. Serum was collected at 24 h after the SAH model with or without AMD3100 or L-NIL treatment. The activity levels of the inflammatory cytokines: (a) IL-1β, (b) IL-6, and (c) TNF-α were measured using ELISA kits. *P < 0.05, **P < 0.01, and ***P < 0.001 versus Vehicle group, each group set contained 6 samples (n=6). The brain sections were obtained from Sham, SAH+Vehicle, SAH+AMD3100, SAH+L-NIL, and

SAH+AMD3100+L-NIL groups respectively at 24h after SAH to performed FJB (d) and Nissl (f) staining. (e) The data represented the quantity of FJB+ cells per square millimeter; **P < 0.01 and ***P < 0.001 versus Vehicle group; the scale bars represent 100 μm and 20 μm, respectively.

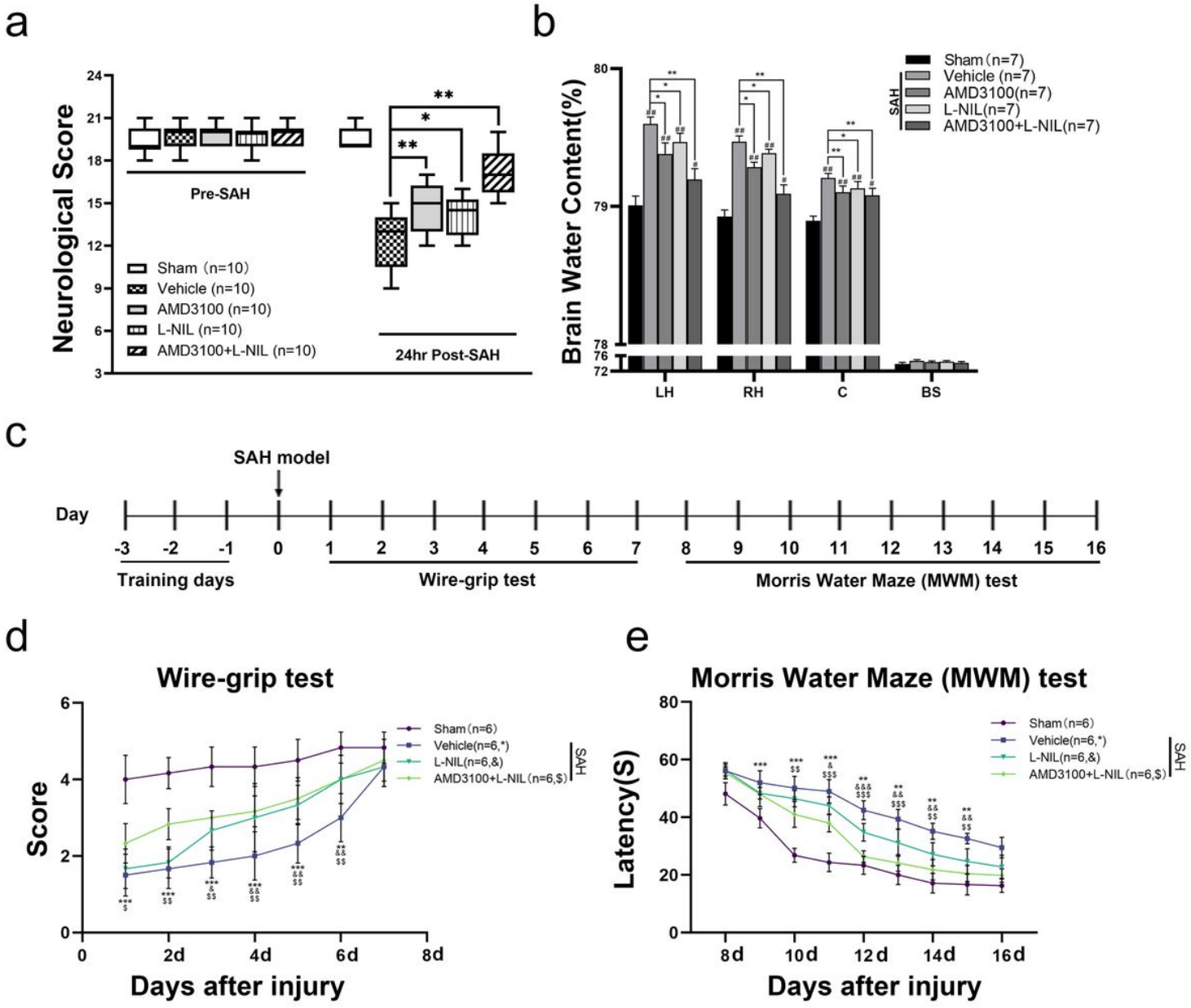

Figure 9

The effect of AMD3100 and L-NIL on neurological functions and brain water content at 24 hours after SAH. At 24 hours following SAH, (a) AMD3100 and L-NIL improved neurological functions (each group set contained 10 samples; n=10), and (b) reduced brain edema (each group set contained 7 samples; n=7). Box=25th-75th interquarile percentiles, horizontal line=median, vertical line=range or Error bars represent mean ± standard error of the mean. AMD3100 and L-NIL decreased SAH-induced behavioral deficits. *P < 0.05 and **P < 0.01 versus Vehicle group, #P < 0.05 and ##P < 0.01 versus Sham group. (c) Experimental flow graph of behavioral tests. Rats were divided into 5 groups: Sham, SAH+Vehicle,

SAH+AMD3100, SAH+L-NIL and SAH+AMD3100+L-NIL to perform behavioral tests. (d) The wire-grip test was first tested on days 1-7, and (e) the Morris Water Maze (MWM) test was performed on days 8-16 post-SAH (each group set contained 6 samples; n = 6). **P < 0.01and ***P < 0.001 versus Sham group; for L-NIL group: &P<0.05, &&P <0.01 and &&&P <0.001 versus Vehicle group; for AMD3100 and L-NIL group: $P <0.05,

$$P < 0.01, and$$

$P < 0.001versus Vehicle group.

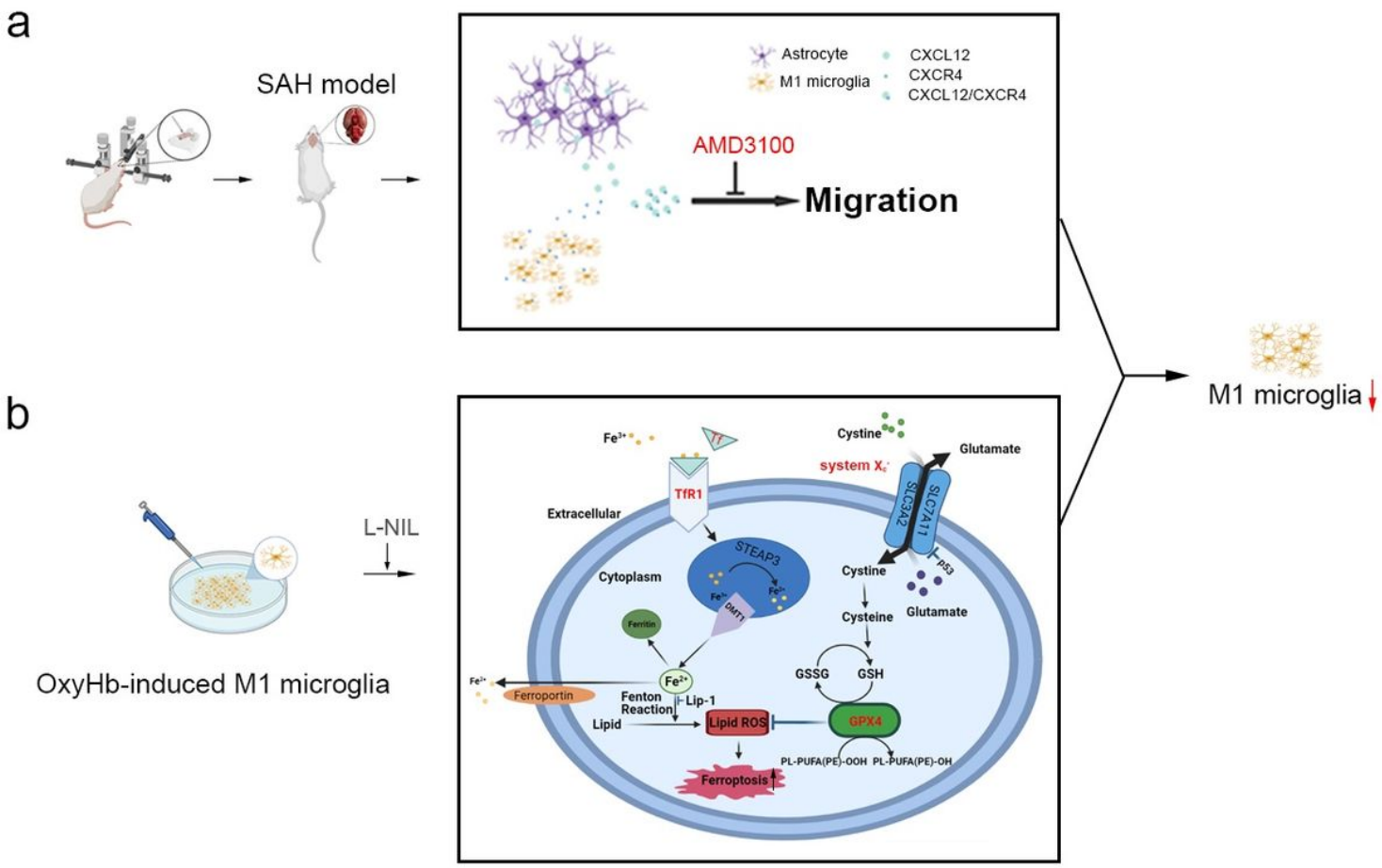

Figure 10

The mechanism of M1 microglia decreasing after SAH. (a) The schematic of M1 microglia migration. (b) The schematic of M1 microglia ferroptosis.

Supplementary Files

This is a list of supplementary files associated with this preprint. Click to download.

- SupplementTable.docx